scientific reports

Check for updates

OPEN

Extreme diversity of 12 cations in folding ALS-linked hSOD1 unveils novel hSOD1-dependent mechanisms for Fe^{2+}/Cu^{2+}-induced cytotoxicity

Liangzhong Lim[1,2], Jian Kang[1,2] & Jianxing Song[1]✉

153-Residue copper-zinc superoxide dismutase 1 (hSOD1) is the first gene whose mutation was linked to FALS. To date, >180 ALS-causing mutations have been identified within hSOD1, yet the underlying mechanism still remains mysterious. Mature hSOD1 is exceptionally stable constrained by a disulfide bridge to adopt a Greek-key β-barrel fold that accommodates copper/zinc cofactors. Conversely, nascent hSOD1 is unfolded and susceptible to aggregation and amyloid formation, requiring Zn^{2+} to initiate folding to a coexistence of folded and unfolded states. Recent studies demonstrate mutations that disrupt Zn^{2+}-binding correlate with their ability to form toxic aggregates. Therefore, to decode the role of cations in hSOD1 folding provides not only mechanistic insights, but may bear therapeutic implications for hSOD1-linked ALS. Here by NMR, we visualized the effect of 12 cations: 8 essential for humans (Na^{+}, K^{+}, Ca^{2+}, Zn^{2+}, Mg^{2+}, Mn^{2+}, Cu^{2+}, Fe^{2+}), 3 mimicking zinc (Ni^{2+}, Cd^{2+}, Co^{2+}), and environmentally abundant Al^{3+}. Surprisingly, most cations, including Zn^{2+}-mimics, showed negligible binding or induction for folding of nascent hSOD1. Cu^{2+} exhibited extensive binding to the unfolded state but led to severe aggregation. Unexpectedly, for the first time Fe^{2+} was deciphered to have Zn^{2+}-like folding-inducing capacity. Zn^{2+} was unable to induce folding of H80S/D83S-hSOD1, while Fe^{2+} could. In contrast, Zn^{2+} could trigger folding of G93A-hSOD1, but Fe^{2+} failed. Notably, pre-existing Fe^{2+} disrupted the Zn^{2+}-induced folding of G93A-hSOD1. Comparing with the ATP-induced folded state, our findings delineate that hSOD1 maturation requires: (1) intrinsic folding capacity encoded by the sequence; (2) specific Zn^{2+}-coordination; (3) disulfide formation and Cu-load catalyzed by hCCS. This study unveils a previously-unknown interplay of cations in governing the initial folding of hSOD1, emphasizing the pivotal role of Zn^{2+} in hSOD1-related ALS and implying new hSOD1-dependent mechanisms for Cu^{2+}/Fe^{2+}-induced cytotoxicity, likely relevant to aging and other diseases.

Amyotrophic lateral sclerosis (ALS) is the most prominent adult motor-neuron disease, clinically characteristic of progressive motor-neuron loss in the spinal cord, brainstem, and motor cortex, which leads to paralysis and death within a few years of onset. ALS was first described in 1869, which affects approximately 1–2 per 100,000 people worldwide[1–4]. Most ALS cases are sporadic (90%) (SALS) whereas 10% are familial ALS (FALS). In 1993, CuZn-superoxide dismutase (SOD1) was identified to be the first gene associated with FALS[4], and its mutations cause the most prevalent form of FALS, accounting for ~ 20% of total FALS cases[4–10]. SOD1 is ubiquitously expressed in all tissues and is the most abundant protein in neurons comprising ~1% of total protein. Currently, > 180 mutations have been identified within the 153-residue human (hSOD1) that cause ALS by gain of toxicity (http://alsod.iop.kcl.ac.uk/)[11]. Interestingly, aggregation of wild-type (WT) hSOD1, without any mutations, has been also observed in SALS patients[12–14]. For example, misfolded wild-type SOD1 has been detected in the cerebrospinal fluid (CSF) of SALS cases. In particular, CSF samples containing misfolded SOD1 showed significant toxicity to motor neuron-like NSC-34 cells[12]. Consequently, the misfolding of wild-type SOD1 in CSF might be a common pathological process in ALS cases. Nevertheless, it still remains controversial whether WT-SOD1 can cause SALS

[1]Department of Biological Sciences, Faculty of Science, National University of Singapore, Singapore 119260, Republic of Singapore. [2]These authors contributed equally: Liangzhong Lim and Jian Kang. ✉email: dbssjx@nus.edu.sg

because the existing data could not completely exclude the possibility that misfolded SOD1 might represent a general consequence of aging and disease[13, 15]. So far, the molecular mechanisms underlying hSOD1-associated ALS still remain a mystery.

hSOD1 represents one of the most studied proteins not only for its physiological and pathological roles, but also for the fundamental principles of the enzymatic catalysis, protein folding and aggregation as well as the modulation by metalation[4–9]. The mature hSOD1 is a homodimeric enzyme of remarkably high stability and solubility, with each subunit folding into an eight-stranded Greek-key β-barrel stabilized by an intramolecular disulfide bridge Cys57-Cys146. Each subunit holds one copper and one zinc ions in close proximity. While zinc ion is coordinated by His63, His71, His80, and Asp83, copper ion is ligated by His46, His48, and His120[4–9] (Fig. 1A). Previous studies have established that nascent hSOD1 without metal cofactors and the disulfide bridge folds into the mature form through a very complex multi-step maturation process, whose detailed mechanism still remains to be completely elucidated. Nevertheless, it has been well recognized that the critical first step of the maturation is the initial folding of nascent hSOD1 specifically induced by Zn^{2+}, which is followed by the formation of the disulfide bridge and incorporation of copper, both of which need the catalysis by copper chaperone for hSOD1 (CCS)[16–19]. In contrast to mature hSOD1 of very high solubility, the early folding species particularly nascent hSOD1 are disordered and have very high tendency of aggregation both in vivo and in vitro[4–9, 17–21]. Consequently, various super-stable hSOD1 mutants with four Cys residues differentially mutated to Ala or/and Ser have been extensively used for biophysical and NMR structural studies[5–8, 22, 23], including the pseudo-WT C6A/C111S mutant whose NMR structure was determined at pH 5.0[22].

Previously, we have obtained atomic-resolution NMR evidence that L126Z-hSOD1, which has the C-terminal 28 residues truncated and considerably elevated toxicity compared to those with site substitution, was highly disordered without any stable secondary and tertiary structures, as well as lacking of restricted ps-ns backbone motions[24]. We further found that nascent hSOD1 was also similarly disordered as L126Z-hSOD1[25], thus providing a biophysical rationale for the observation that WT-hSOD1 might be associated with SALS[12–14]. Furthermore, we found that while nascent WT-hSOD1 could bind Zn^{2+} to undergo the initial folding into the co-existence between the folded and unfolded states at 1:20[25], L126Z-hSOD1 completely lost the ability to interact with Zn^{2+} to fold[24]. In the absence of Zn^{2+}, nascent hSOD1 is also able to interact with membrane mimics including micelle and bicelle. Nevertheless, upon availability of Zn^{2+}, nascent hSOD1 becomes co-existing between two states and no longer able to interact with membrane mimics, while L126Z-hSOD1 remains disordered and still interacting with membrane mimics[24, 25]. Remarkably, in vivo studies revealed that the ALS-causing mutants of hSOD1 did

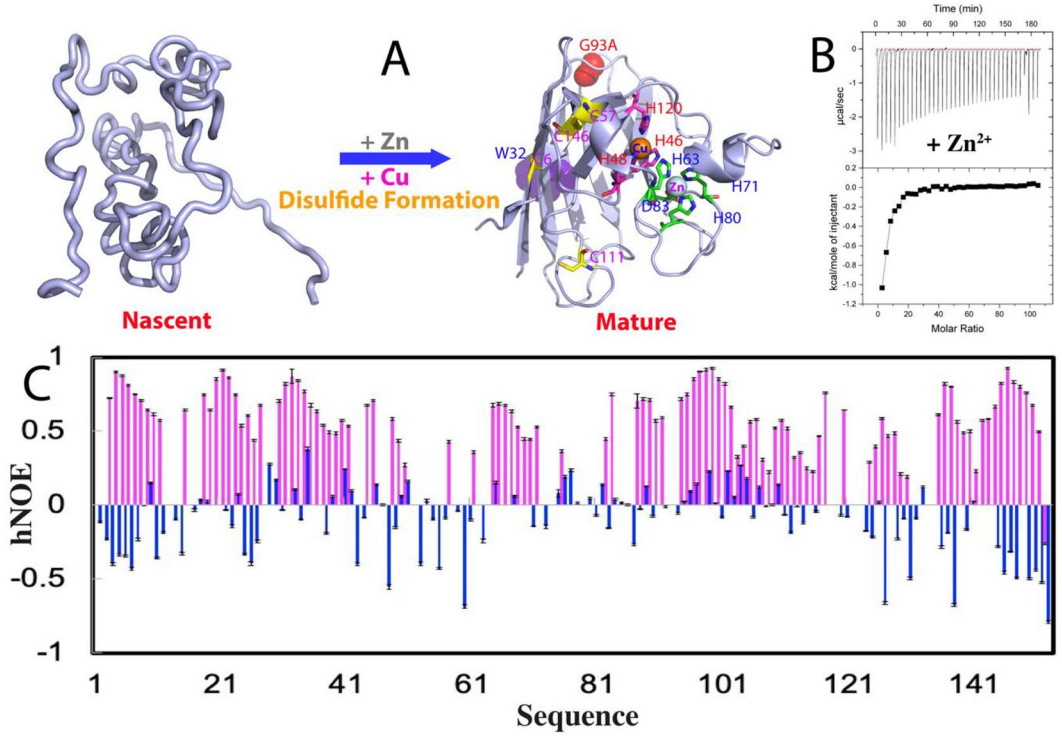

Figure 1. ITC and NMR characterization of the Zn^{2+}-induced folding of nascent hSOD1. (**A**) Schematic representation of the folding of nascent hSOD1 into the folded subunit. The folded hSOD1 is represented by the monomer of the dimeric crystal structure of hSOD1 (1PU0). Residues for binding zinc and copper are labeled. (**B**) (Upper) ITC profiles of the interactions of the unfolded hSOD1 state with Zn^{2+}, and (Lower) integrated values for reaction heats with subtraction of the corresponding blank results normalized against the amount of ligand injected versus the molar ratio of hSOD1: Zn^{2+}. (**C**) $\{^1H\}$–^{15}N heteronuclear steady-state NOE (hNOE) of nascent hSOD1 (blue) and Zn^{2+}-induced folded state (purple).

initiate ALS pathogenesis by becoming associated with the ER and mitochondria membranes[26]. Very recently, a biophysical study showed that the disruption of the ability of hSOD1 by ALS-causing mutations to bind Zn^{2+} is correlated to the acquired ability to become associated with mitochondria membrane to further form toxic aggregates[27]. These results together highlight the extreme criticality of the initial folding of nascent hSOD1 induced by Zn^{2+}, implying that the failure to achieve the initial folding may render WT-hSOD1 to become as toxic as the ALS-causing mutants, thus representing a convergent mechanism for the mutant hSOD1 to cause FALS and WT-hSOD1 to trigger SALS. On the other hand, accumulation of iron and copper within CNS has been extensively identified in ALS cases[28–31]. In particular, it has been revealed that in the SOD1-G93A mice, the breakdown of blood–spinal cord barrier (BSCB) in the early ALS disease phase led to accumulation of blood-derived iron in the spinal cord, which initiates ALS by triggering early motor-neuron degeneration through iron-induced oxidant stress[31]. In this context, two questions of both fundamental and therapeutic importance arise: (1) in addition to Zn^{2+}, are other cations also able to induce the initial folding of nascent hSOD1? (2) is hSOD1 involved in the manifestation of Fe^{2+}-/Cu^{2+}-induced cytotoxicity?

In this study, we aimed to address the two questions by NMR. Briefly we have selected and evaluated the effects of 12 inorganic cations (Fig. S1), which include 8 (Na^{+}, K^{+}, Ca^{2+}, Zn^{2+}, Mg^{2+}, Mn^{2+}, Cu^{2+}, and Fe^{2+}) essential for humans[32], 3 (Ni^{2+}, Cd^{2+} and Co^{2+}) widely thought to have physicochemical properties very similar to Zn^{2+} and thus extensively used to mimic Zn^{2+} in structure determination[5–8], as well as environmentally abundant Al^{3+}. Surprisingly, most cations show no detectable ability to bind or to induce folding of nascent hSOD1 even up to a molar ratio of 1:40 (hSOD1:cation) beyond which the sample started to precipitate. Intriguingly, Cu^{2+}, the catalytic cofactor of hSOD1, shows extensive binding to the unfolded state but triggers severe aggregation. Unexpectedly for the first time, Fe^{2+} has been identified to have the Zn^{2+}-like capacity to induce folding. Subsequently, we further characterized the effect of Fe^{2+} on the Zn^{2+}-binding-defective H80S/D83S-hSOD1 as well as ALS-causing G93A-hSOD1 mutants. Very surprisingly, H80S/D83S-hSOD1 no longer undergoes the Zn^{2+}-induced folding as expected but can still be induced to fold by Fe^{2+}. Conversely, Zn^{2+} retains its ability to initiate folding of G93A-hSOD1, whereas Fe^{2+} loses this capacity. Notably, the pre-existence of Fe^{2+} significantly disrupts the capacity of Zn^{2+} to induce the initial folding of G93A-hSOD1. These results together indicate that although the Zn^{2+}- and Fe^{2+}-binding pockets might be only overlapped, either binding is sufficient to induce folding of nascent hSOD1.

Recently, we discovered that ATP and triphosphate could induce the initial folding of nascent hSOD1, while ADP, Adenosine, pyrophosphate and phosphate, as well as TMAO had no detectable inducing activity[33]. By comparing with the ATP-induced folded state of hSOD1, the present results decipher that hSOD1 maturation at least requires: (1) intrinsic folding capacity encoded by the sequence; (2) additional information specifically provided by the Zn^{2+}-coordination and; (3) disulfide formation and copper-load catalyzed by hCCS. Therefore, the study not only unveils the biophysical basis for the irreplaceable roles of Zn^{2+} in inducing the initial folding of nascent hSOD1 and thus in preventing ALS pathogenesis, but also uncovers new hSOD1-dependent mechanisms for Cu^{2+}-/Fe^{2+}-induced cytotoxicity.

Results

NMR characterization of the effect of Zn^{2+} on nascent hSOD1 and its H80S/D83S mutant

Previously it has been shown that even in cells, four cysteines of WT hSOD1 could form intermolecular disulfide-scrambled aggregates which might be associated with ALS[34–36]. Furthermore, even the pseudo-WT C6A/C111S mutant formed intermolecular disulfide-scrambled aggregates at pH above 5.0, and consequently its NMR structure was determined at pH 5.0[22]. As such, in the current study, all biophysical experiments on WT hSOD1, which possesses all four cysteines, were carried out in a 1 mM acetate buffer at pH 4.5 in order to both minimize intermolecular disulfide-scrambled aggregation observed during the experiments and maximally manifest the effects of 12 titrated cations on the binding and folding of nascent hSOD1.

As shown in Fig. S2A, nascent hSOD1 with the wild-type sequence is highly unfolded, which has an HSQC spectrum with very narrow ^{1}H and ^{15}N spectral dispersions typical of a highly disordered protein. This observation aligns with the previous findings for WT-hSOD in cell[18,19], but is different from the results obtained in vitro with various super-stable hSOD1 mutants. In these mutants, four Cys residues (Cys 6, Cys 57, Cys 111, and Cys 146) were differentially replaced to enhance stability and inhibit aggregation. For instance, the pseudo-WT mutant C6A/C111S was found to be partially folded even in the absence of Zn^{2+} ions and the disulfide bridge[5–8,22,23].

As monitored by isothermal titration calorimetry (ITC), the heat release was observed upon adding Zn^{2+} (Fig. 1B), indicating that Zn^{2+} could indeed interact with nascent hSOD1. However, as the heat changes are expected to result from at least two processes: namely binding of Zn^{2+} to hSOD1 and binding-induced folding, data fitting is not possible to obtain the thermodynamic parameters for the binding event. Consistent with ITC results, upon adding Zn^{2+}, a folded population was formed as unambiguously indicated by the manifestation of a new set of well dispersed HSQC peaks (Fig. S2B). The formation of the folded state is largely saturated at a ratio of 1:20 (hSOD1: Zn^{2+}) and even with further addition of Zn^{2+} up to 1:40 (hSOD1: Zn^{2+}), the unfolded and folded states still coexist[25], suggesting that Zn^{2+} alone is insufficient to completely convert the unfolded population into the folded state, consistent with the in-cell results that the complete formation of the mature WT-hSOD1 structure needs further disulfide formation and copper-load that is catalyzed by human copper chaperone for hSOD1 (hCCS)[17–19]. Remarkably, upon adding EDTA at an equal molar concentration of Zn^{2+}, the well-dispersed peaks of the folded state became completely disappeared, confirming that the formation of the folded state is the Zn^{2+}-induced effect[25].

As shown in Fig. S2C, all residues of nascent hSOD1 have very small absolute values of ($\Delta C\alpha - \Delta C\beta$) chemical shifts, indicating the absence of any stable secondary structures[37]. By contrast, many residues of the Zn^{2+}-induced

folded state have large and negative (ΔCα−ΔCβ) (Fig. S2C), which are highly similar to those of the Zn^{2+}-induced state of the pseudo-WT hSOD1 C6A/C111S except for several residues close to the mutation sites (Fig. S2D). The results together suggest that in the presence of Zn^{2+}, both nascent WT and pseudo-WT hSOD1 adopt the highly similar β-barrel structures (Fig. S2E). Nevertheless, upon induction by Zn^{2+}, all population of the pseudo-WT hSOD1 became folded with a well-defined three-dimensional structure (Fig. S2E) as determined by NMR[22], which is very similar to the crystal structure of the mature hSOD1[38]. By contrast, WT-hSOD1 still has a co-existence of the unfolded and folded populations in the presence of an excess amount of Zn^{2+}.

We further obtained $\{^1H\}-^{15}N$ heteronuclear steady-state NOE (hNOE) of the folded and unfolded states of hSOD1 in the presence of Zn^{2+} at 1:20 (hSOD1: Zn^{2+}) (Fig. 1C), which reflects the backbone motion on ps-ns time scale[33, 39–41]. The residues of the unfolded state have small or even negative hNOE values with an average of −0.11, indicating that the unfolded state undergoes largely unrestricted backbone motions on ps-ns time scale. By contrast, most residues of the folded state have positive hNOE values with an average of 0.61, while some are even higher than 0.8, implying that the folded state has highly restricted backbone motions on ps-ns time scale. However, the average hNOE value of the folded state is much smaller than that of a well-folded protein such as EphA4 receptor[40], but similar to that of C71G-hPFN1[33] and the N-terminal domain of the ALS-causing TDP-43[41], which also have co-existing unfolded and folded conformations. Here, we further collected ^{15}N-edited HSQC-NOESY spectrum on the sample with the coexistence of the unfolded and folded states of hSOD1 but unlike the C71G-hPFN1[33] and N-terminal domain of TDP-43[41], we found no NOE cross-peaks resulting from the exchange between two states, indicating that the time scale for the conformational exchange is slower than that for the C71G-hPFN1 (~ 12 Hz) and TDP-43 N-Domain (~ 14 Hz)[33, 40–42].

We also generated the H80S/D83S-hSOD1 mutant, which was previously shown to have severely-abolished capacity in Zn^{2+}-binding[43]. As shown in Fig. 2A, this mutant is also highly-disordered in the nascent form like the wild-type hSOD1, as evident by its poorly-dispersed HSQC spectrum with most peaks superimposable to those of the wild-type except for those of mutated residues and several residues close to the mutation sites in sequence.

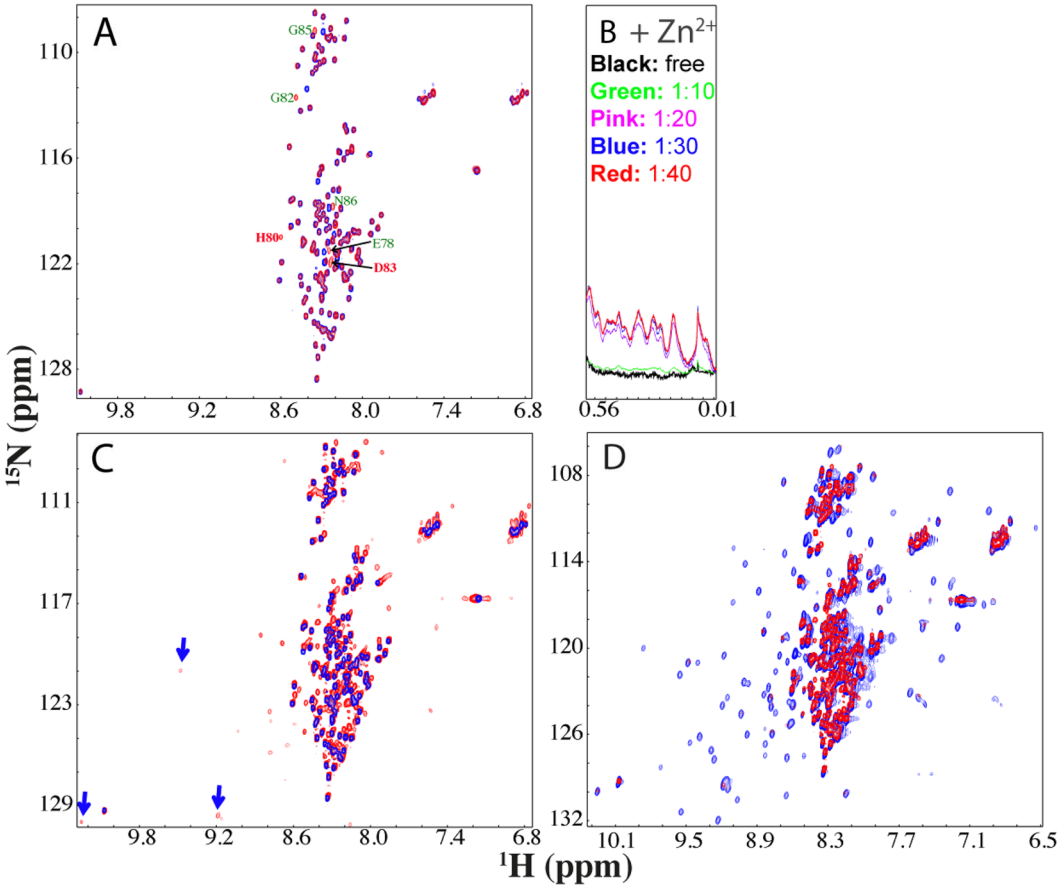

Figure 2. NMR characterization of the interaction of the H80S/D83S-hSOD1 with Zn^{2+}. (**A**) Superimposition of HSQC spectra of the WT nascent hSOD1 (red) and H80S/D83S mutant (blue). Residues with large differences for their HSQC peaks are labeled. (**B**) Up-field 1D NMR peaks characteristic of the folded form of H80S/D83S (0.0–0.6 ppm) induced by the presence of Zn^{2+} at different molar ratios. (**C**) Superimposition of HSQC spectra of H80S/D83S in the absence (blue) and in the presence of Zn^{2+} at a molar ratio of 1:40 (red). Some well-dispersed peaks characteristic of the partially-folded form are indicated by blue arrows. (**D**) Superimposition of HSQC spectra of the WT hSOD1 in the presence of Zn^{2+} at a molar ratio of 1:20 (blue), and H80S/D83S in the presence of Zn^{2+} at a molar ratio of 1:40 (red).

Indeed, upon addition of Zn^{2+} at a ratio of 1:10 (H80S/D83S:Zn^{2+}), only very minor change was observed for the up-field 1D peaks (Fig. 2B) and the changes were mostly saturated at 1:30. However, even at a ratio of 1:40, the majority of well-dispersed HSQC peaks characteristic of the well-folded hSOD1 is not detected (Fig. 2C). Nevertheless, several relatively-dispersed HSQC peaks of the mutant in the presence of Zn^{2+} manifested and are mostly superimposable to those of the Zn^{2+}-bound WT hSOD1 (Fig. 2D). The results together indicate that the mutations significantly reduce the zinc-binding capacity as previously shown[43]. Consequently, for this double mutant, even the excess supplement of Zn^{2+} could only trigger the formation of the partially-folded form, thus implying that the Zn^{2+}-induced folding is not just due to non-specific electrostatic/salt effects, but results from highly specific interactions between Zn^{2+} and hSOD1 residues.

Copper extensively binds but triggers severe aggregation

We subsequently assessed whether copper, the catalytic cofactor of hSOD1, can bind and induce folding of nascent hSOD1. Intriguingly, on the one hand, as shown in Fig. 3A, Cu^{2+} induced extensive shift and broadening of HSQC peaks of the unfolded state. On the other hand, however, unlike Zn^{2+} which was capable of inducing the manifestation of a complete set of well-dispersed HSQC peaks from the folded state, Cu^{2+} only induced the formation of a partially-folded state as indicated by the observations that only several well-dispersed HSQC peaks (Fig. 3A) and very up-field 1D peaks (Fig. 3B) manifest such as that of Trp32 side chain which are from the folded state. The fact that most well-dispersed HSQC peaks characteristic of the Zn^{2+}-induced folded state were undetectable implies that a large region of the Cu^{2+}-induced state is not well-folded, or/and undergoes μs-ms conformational exchanges. Interestingly, the Cu^{2+}-induced effect was mostly saturated at 1:6 (hSOD1:Cu^{2+}) as evidenced by the very up-field 1D spectra. The current NMR results are generally consistent with the very recent report that unlike Zn^{2+}, Cu^{2+} has no ability to prevent nascent hSOD1 from interacting with membrane to form toxic aggregates[23], implying that Cu^{2+} has no strong capacity to induce the initial folding of nascent hSOD1, which is required for abolishing the membrane-interacting ability.

We also observed that even upon immediate addition of Cu^{2+}, hSOD1 appeared to undergo μs-ms conformational exchanges or/and dynamic aggregation as evidenced by very broad 1D and HSQC peaks as compared with those in the presence of Zn^{2+} (Fig. 3A,B). Particularly after one hour, the NMR sample in the presence of Cu^{2+} started to form visible aggregates and consequently all NMR signals became disappeared. Consistent with this observation, addition of EDTA to the hSOD1 sample with freshly-added Cu^{2+} could result in the disappearance of very up-field 1D peaks and well-dispersed HSQC peaks, as well as the shifts of HSQC peaks, indicating that the observed effects are specifically induced by Cu^{2+}. However, addition of EDTA to the Cu^{2+}-added hSOD1 sample which already had visible aggregates failed to solubilize the aggregates as well as to restore the disappeared HSQC peaks, implying that the aggregation is highly irreversible.

We managed to conduct ITC titrations of Cu^{2+} into nascent hSOD1 sample at a low protein concentration (5 μM) and the result indicated that Cu^{2+} indeed showed the binding (Fig. 3C). Intriguingly, we also added Cu^{2+} to the hSOD1 sample in the pre-existence of Zn^{2+} at 1:20, but unfortunately the sample got precipitated immediately. In this context, the extensive binding of Cu^{2+} to the unfolded state, inability to induce the well-folded form, and strong induction of aggregation by Cu^{2+} may partly account for its high in vivo toxicity and also rationalize why the delivery and load of copper needs to be specifically implemented by hCCS to the pre-folded hSOD1 population[16–19].

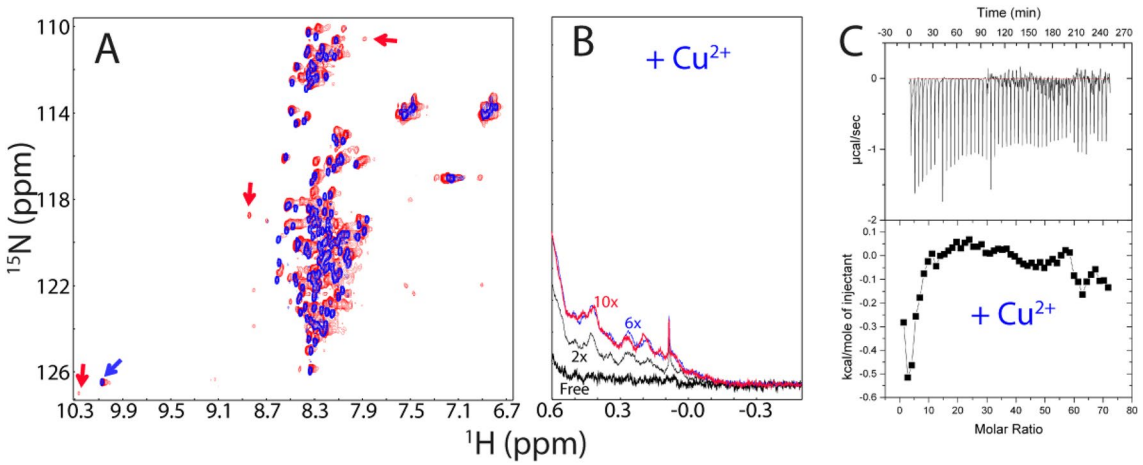

Figure 3. Cu^{2+} extensively binds the unfolded hSOD1 ensemble. (**A**) Superimposition of HSQC spectra of hSOD1 in the absence (blue) and in the presence of Cu^{2+} at a molar ratio of 1:10 (red). The blue arrow is used for indicating the HSQC peak of Trp32 ring proton characteristic of the unfolded ensemble and red ones for some HSQC peaks characteristic of the partially-folded form. (**B**) The up-field 1D NMR peaks characteristic of the partially-folded hSOD1 (−0.5 to 0.62 ppm) in the absence and in the presence of Cu^{2+} at different molar ratios. (**C**) (Upper) ITC profiles of the interactions of the unfolded hSOD1 state with Cu^{2+}, and (Lower) integrated values for reaction heats with subtraction of the corresponding blank results normalized against the amount of ligand injected versus the molar ratio of hSOD1: Cu^{2+}.

Most cations show no capacity in binding and inducing folding

So, a question of fundamental and biological interest is whether metal cations other than Zn^{2+} and Cu^{2+} can also bind and induce folding of nascent hSOD1. Previously, other metal cations have been extensively demonstrated to be capable of substituting either zinc or/and copper ions in mature hSOD1[5–7] but it remains completely unknown whether they have the Zn^{2+}-like capacity in triggering the folding of nascent hSOD1. To address this, we have further selected 10 other cations from the periodic table (Fig. S1), which include Na^{+}, K^{+}, Ca^{2+}, Mg^{2+}, Mn^{2+}, Fe^{2+}, Ni^{2+}, Cd^{2+}, Co^{2+} and Al^{3+} and subsequently conducted titrations into nascent hSOD1 with ratios of cation:hSOD1 reaching up to 1:40 (hSOD1: cation) under the exactly same protein concentration and solution conditions used for Zn^{2+} as monitored by NMR HSQC spectroscopy, which can detect the binding events at residue-specific resolution with affinities ranging from very high to very low events even with Kd of mM[31,44,45].

Very unexpectedly, except for Fe^{2+}, all cations triggered no considerable shift of HSQC peaks and no manifestation of very up-field 1D and well-dispersed HSQC peaks for nascent hSOD1, as exemplified by the results with Co^{2+}, Ni^{2+}, Cd^{2+}, and Mn^{2+} which induce no large shift of HSQC peaks of nascent hSOD1 even with the ratio reaching up to 1:40 (hSOD1: cation) (Fig. 4), thus suggesting that these cations have no capacity to bind as well as to induce folding of nascent hSOD1. This is remarkably surprising because previously in various biophysical investigations and structure determinations, Ni^{2+}, Cd^{2+} and Co^{2+} have been widely thought to have physicochemical properties very similar to Zn^{2+} and thus used to substitute Zn^{2+} in the mature hSOD1[5–7]. The present results indicate that not all cations capable of binding to the mature hSOD1 can bind or induce folding of nascent hSOD1, thus strongly highlighting the irreplaceable role of Zn^{2+} in initiating the first step of the maturation: folding of nascent hSOD1. Indeed, previous folding studies have deciphered that zinc appears to uniquely modulate the entire folding free energy surface of hSOD1[46].

So, an intriguing question arises: why does the WT hSOD1 still retain equilibrium between the folded and unfolded forms even in the excess presence of Zn^{2+}? Previous studies revealed a surprising fact that on the one hand, to achieve copper-load and disulfide formation catalyzed by hCCS, the hSOD1 needs to populate the folded form bound to Zn^{2+} to some degree. Otherwise, the efficacy of maturation was low, as exemplified by the mutants[5–7,46–48]. On the other hand, the interaction between hCCS and folded hSOD1 cannot be too stable but has to be dynamic/transient. If the SOD1-hCCS complex is too stable, the efficiency of the hCCS-catalyzed

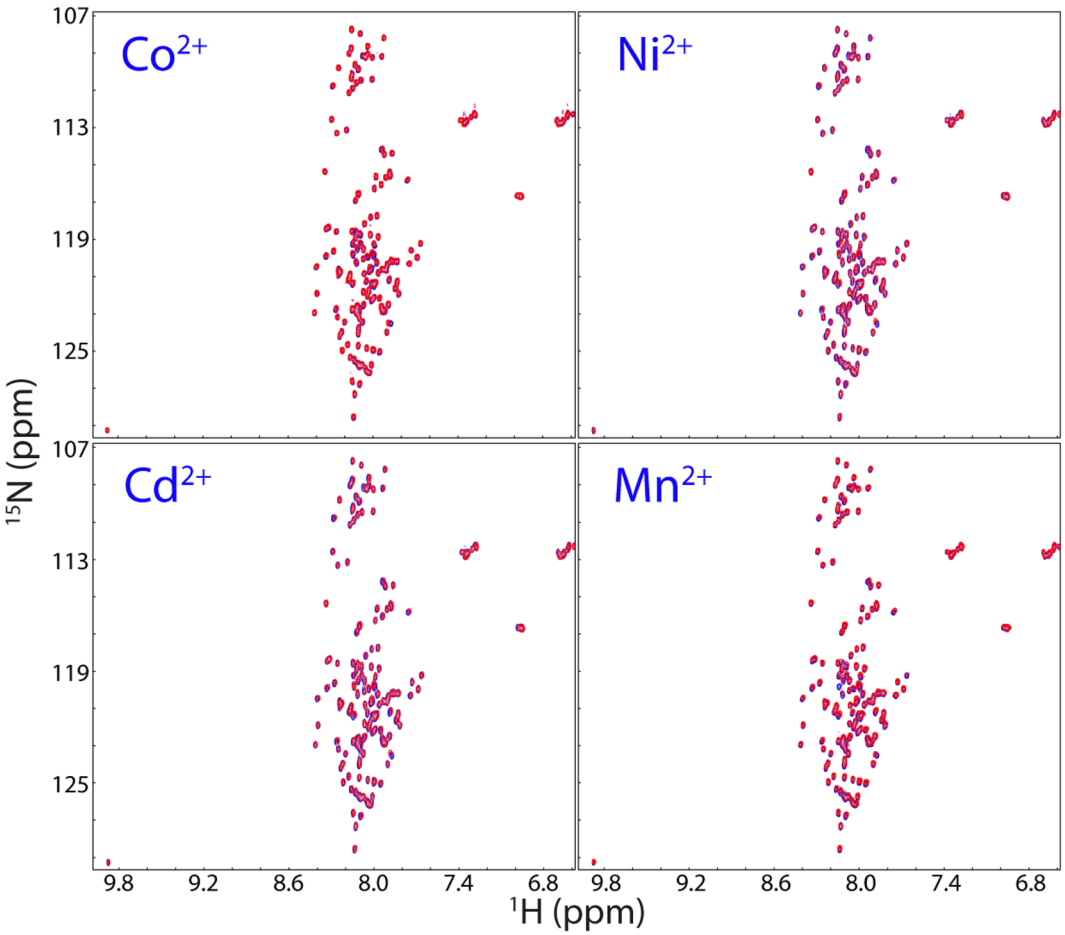

Figure 4. HSQC characterization of interactions of nascent hSOD1 with four cations. Superimposition of HSQC spectra of nascent hSOD1 (blue) and in the presence of Co^{2+}, Ni^{2+}, Cd^{2+}, and Mn^{2+} respectively at a molar ratio of 1:40 (red).

maturation will also be reduced or even abolished[48]. So, the request for dynamic/transient interactions between hSOD1 and hCCS appears to be elegantly fulfilled by the dynamic nature of the immature SOD1, which at least partly results from the co-existence of the unfolded and folded population in the presence of Zn^{2+}.

Fe^{2+} induces folding of nascent hSOD1

Here by a systematic assessment, for the first time we found that most unexpectedly, Fe^{2+} owns the capacity in triggering folding of nascent hSOD1 into an equilibrium between the unfolded and Fe^{2+}-induced folded states. So, we subsequently conducted a detailed NMR characterization to elucidate its conformational features. As seen in Fig. 5A, addition of Fe^{2+} triggered the manifestation of very up-field 1D and well-dispersed HSQC peaks characteristic of the folded form and the increase in the folded population is mostly saturated at a molar ratio of 1:20 (hSOD1: Fe^{2+}). Figure 5B presents the superimposition of the HSQC spectra of the Fe^{2+}- and Zn^{2+}-bound hSOD1 forms. Unfortunately, a detailed comparison of the intensities and chemical shifts of NMR peaks induced by Fe^{2+} and Zn^{2+} is impossible because Fe^{2+} has strong paramagnetic effects including effects of relaxation enhancement and pseudo-contact shift[49], which also made the sequential assignment of the Fe^{2+}-bound state impossible by NMR. However, ITC measurement also revealed that Fe^{2+} could indeed bind hSOD1 (Fig. 5C).

Nevertheless, based on the assignments of the Zn^{2+}-bound form, many peaks from the Fe^{2+}-bound hSOD1 are highly superimposable to those of the Zn^{2+}-induced state; while some have large differences. Interestingly, as shown in Fig. 5D, the peaks with significant differences are from the residues surrounding the Cu/Zn binding pocket, while the peaks without significant differences are from those located relatively far away from the Cu/Zn binding pocket such as over the β-barrel. This observation strongly implies that: (1) the structures of hSOD1 induced by Fe^{2+} and Zn^{2+} may be highly similar, especially in the β-barrel regions, and (2) the Fe^{2+} binding pocket significantly overlaps with the classic Cu/Zn binding pocket. Consequently, the residues close to Fe^{2+} showed large differences for their HSQC peaks due to the pseudo-contact shift effect[49], or/and slightly-different conformations in the Fe^{2+}-induced state. Moreover, the up-field and well-dispersed HSQC peaks also became completely disappeared upon adding EDTA, confirming that the formation of the folded hSOD1 is also Fe^{2+}-induced effect.

We further conducted a competitive experiment between Zn^{2+} and Fe^{2+} by monitoring the changes of both up-field (Fig. 6A) and HSQC (Fig. 6B,C) peaks upon stepwise addition of Zn^{2+} into the hSOD1 sample in the pre-existence of 20 × Fe^{2+}. As seen in Fig. 6A, with addition of 10× zinc, the zinc-specific peak in the 1D spectrum manifested. On the other hand, however, as shown in HSQC spectra (Fig. 6B), in the presence of 10× zinc, many HSQC peaks still remain highly similar to those of the Fe^{2+}- induced state. Upon addition of 20× Zn^{2+}, although many peaks become superimposable to those of Zn^{2+}-bound form, there are still some peaks more superimposable to those of the Fe^{2+}-induced state (Fig. 6C). This implies that Fe^{2+} and Zn^{2+} binding-sites might be only partly overlapped. Unfortunately, further addition of Zn^{2+} induced severe broadening of the NMR peaks and then visible aggregates of the sample, thus blocking further characterization. Nevertheless, the results of the competitive experiment strongly imply that the presence of Fe^{2+} at high concentrations can interfere in the Zn^{2+}-induced formation of the well-folded hSOD1, which may reduce the efficiency of the maturation of WT hSOD1. Intriguingly, we also attempted to add Cu^{2+} into the hSOD sample in the pre-existence of 20× Fe^{2+}. Unfortunately, even the addition of Cu^{2+} at 1:5 (hSOD1:Cu^{2+}) induced severe aggregation of the sample and NMR signal became undetectable.

Characterization of the Zn^{2+}- and Fe^{2+}-binding pockets with hSOD1 mutants

We further titrated the H80S/D83S-hSOD1 mutant with Fe^{2+} by monitoring the changes of up-field 1D (Fig. 7A) and HSQC (Fig. 7B) spectra. Very unexpectedly, although for this mutant, Zn^{2+} was unable to trigger the formation of the well-folded structure (Fig. 2), Fe^{2+} was still able to induce folding as evident from the manifestation of up-field peaks mostly saturated at a ratio of 1:20 (hSOD1:Fe^{2+}) (Fig. 7A), as well as well-dispersed HSQC peaks (Fig. 7B), which are mostly superimposable to those of WT-hSOD1 (Fig. 7C). These results suggest that the Fe^{2+}-induced structures are highly similar for both H80S/D83S mutant and wild-type hSOD1. Crucially, the results also reveal that the residues for binding Zn^{2+} and Fe^{2+} are not identical. Very strikingly, however, either Zn^{2+}- or Fe^{2+}-binding is sufficient to trigger folding of nascent hSOD1.

Fe^{2+} radically disrupts the Zn^{2+}-induced folding of G93A-hSOD1

So far, > 180 ALS-causing mutations have been identified on the 153-residue hSOD1 but it still remains highly elusive for the mechanism by which these mutations cause ALS. To explore this, we generated the ALS-causing G93A-hSOD1 protein, which was also highly disordered like WT as judged by its poorly-dispersed HSQC spectrum (Fig. 8A). Interestingly, however, in addition to the residues such as Asp92, Val94 and Ala95 which are next to the mutation residue Gly93 in sequence, many residues such as Gln22, Glu24, Asp101 and Asp103 far away from Gly93, also showed significant shifts for their HSQC peaks (Fig. 8A). This is very different from what observed on the double mutant H80S/D83S (Fig. 2a), implying that even in the unfolded ensemble, the ALS-causing mutation of G93A is able to trigger long-range perturbations on other residues.

Amazingly, although the G93A mutation is not located within the Zn^{2+}/Cu^{2+} binding pocket, G93A-hSOD1 lost the ability to undergo folding upon induction by Fe^{2+}. Even in the presence of 80× Fe^{2+}, no peaks characterized by the folded form manifested over up-field region (Fig. 8B), and in its HSQC spectrum (Fig. 8C). On the other hand, the presence of Fe^{2+} led to significant shifts of some HSQC peaks of the unfolded state, most of which are from the residues close to the Cu/Zn binding pocket except for Ala4, Leu6, Ile113 and the mutation residue Ala93 (Fig. 8C,D), indicating that Fe^{2+} might bind these residues of the unfolded state but initiated no further folding. However, again due to the paramagnetic nature of Fe^{2+}, it is impossible to correlated these shifts to the solvent exposure, or/and direct binding, or/and binding-induced conformational/dynamic changes of these residues in the unfolded ensemble of G93A-hSOD1.

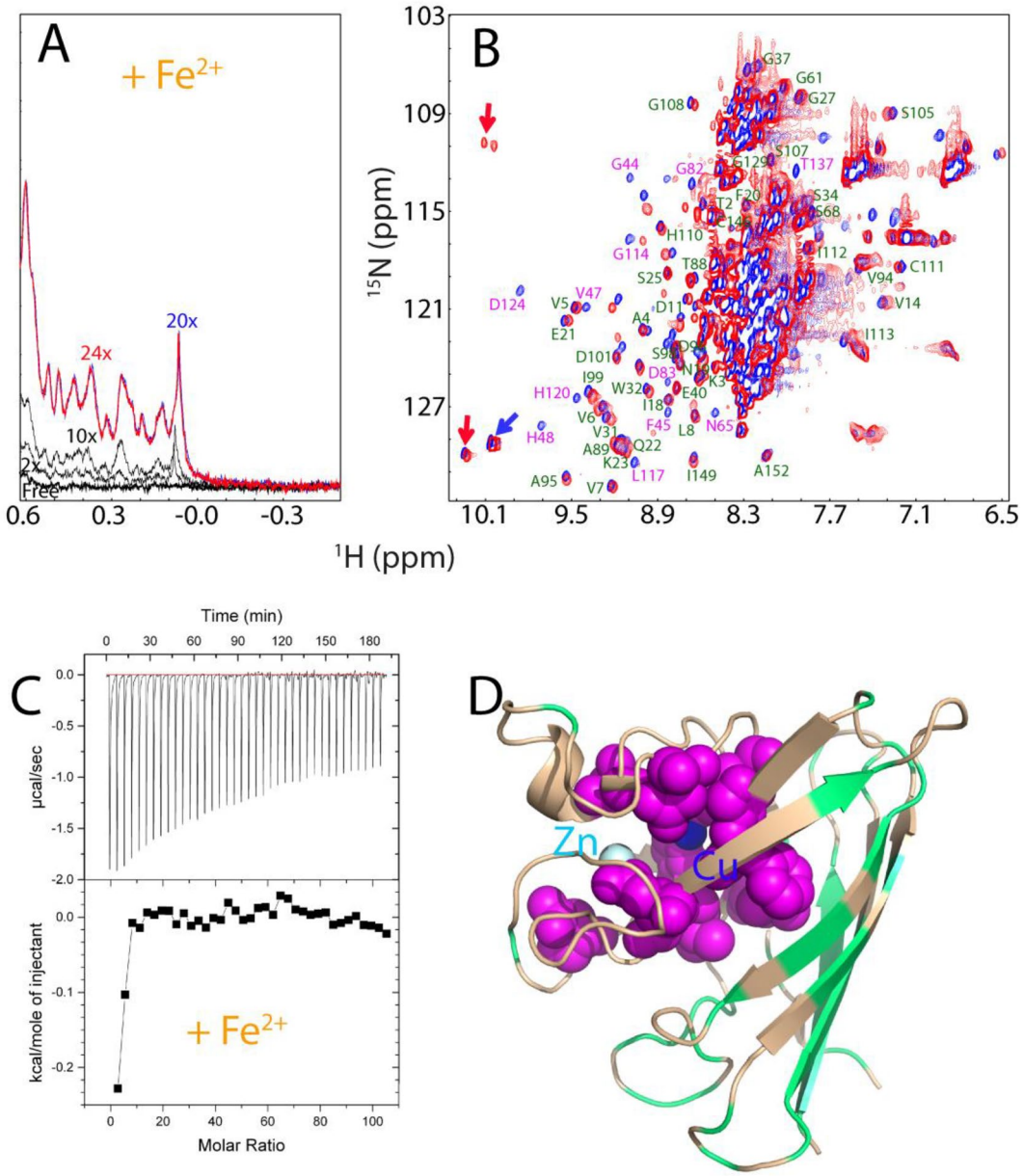

Figure 5. Fe^{2+} has the Zn^{2+}-like capacity in triggering the folding of nascent hSOD1. (**A**) Up-field 1D NMR peaks characteristic of the folded hSOD1 (− 0.5 to 0.62 ppm) in the absence and in the presence of Fe^{2+} at different molar ratios. (**B**) Superimposition of HSQC spectra of hSOD1 in the presence of Zn^{2+} (blue), and Fe^{2+} (red). The labels of the sequential assignments for some well-resolved HSQC peaks are in green if the peaks are largely superimposable but in pink if the peaks are largely shifted in both forms. (**C**) (Upper) ITC profiles of the interactions of the unfolded hSOD1 ensemble with Fe^{2+}, and (Lower) integrated values for reaction heats with subtraction of the corresponding blank results normalized against the amount of ligand injected versus the molar ratio of hSOD1: Fe^{2+}. (**D**) The monomer structure of hSOD1 (1PU0) with the residues displayed in pink spheres if their HSQC peaks showed large differences in the Zn^{2+}- and Fe^{2+}-forms, and colored in green if their HSQC peaks were superimposable.

On the other hand, addition of Zn^{2+} was still able to trigger the formation of the folded state of G93A-hSOD1, as evident from the manifestation of up-field 1D (Fig. 9A) and well-dispersed HSQC peaks (Fig. 9B). However, as compared to the titration results of WT hSOD1 by Zn^{2+}, two significant differences were observed (Fig. 9A). First, at the same ratio, the intensity of up-field peaks of G93A is much lower than that of WT SOD1. Second, the Zn^{2+}-induced formation of the G93A folded state would not become saturated even up to 1:60. However, attempts to further add Zn^{2+} triggered severe aggregation of G93A-hSOD1, thus preventing from further characterization at higher ratios of Zn^{2+}. Nevertheless, both differences imply that the G93A-hSOD1 has a considerably reduced capacity in forming the folded form even induced by Zn^{2+}.

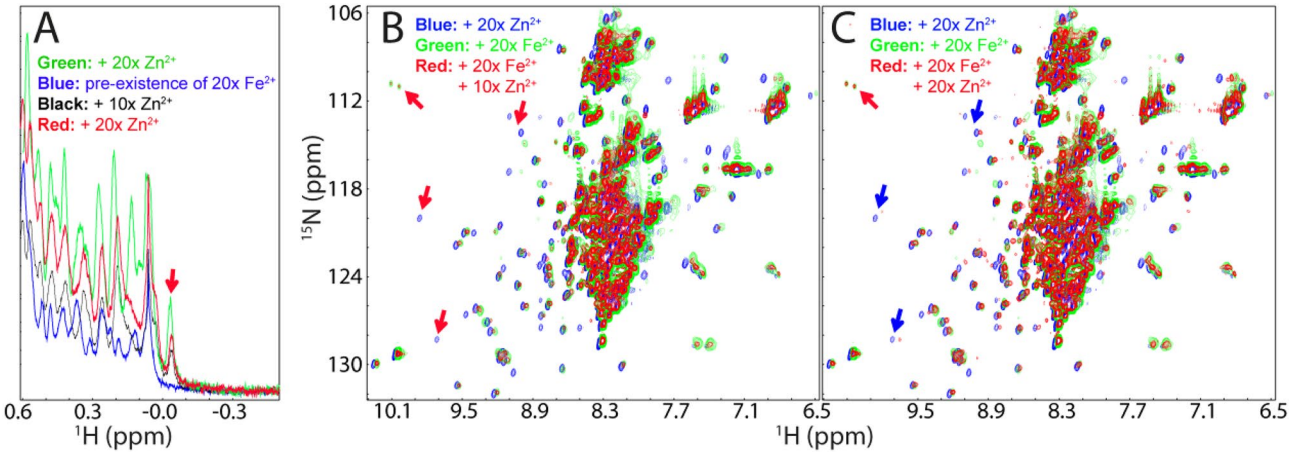

Figure 6. Fe^{2+} and Zn^{2+} have partly overlapped binding sites. (**A**) Up-field 1D NMR peaks (− 0.5 to 0.62 ppm) of hSOD1 in the presence of 20× Zn^{2+} (green), 20× Fe^{2+} (blue), addition of 10× Zn^{2+} into the sample in the pre-existence of 20× Fe^{2+} (black); and addition of 20 × Zn^{2+} into the sample in the pre-existence of 20× Fe^{2+} (red). (**B**) Superimposition of HSQC spectra of hSOD1 in the presence of 20× Zn^{2+} (blue), in the presence of 20× Fe^{2+} (green), and in the presence of both 20× Fe^{2+} and 10× Zn^{2+} (red). (**C**) Superimposition of HSQC spectra of hSOD1 in the presence of 20× Zn^{2+} (blue), in the presence of 20× Fe^{2+} (green), and in the presence of both 20× Fe^{2+} and 20× Zn^{2+} (red). Red arrows are used for indicating Fe^{2+}-specific HSQC peaks while blue arrows for Zn^{2+}-specific peaks.

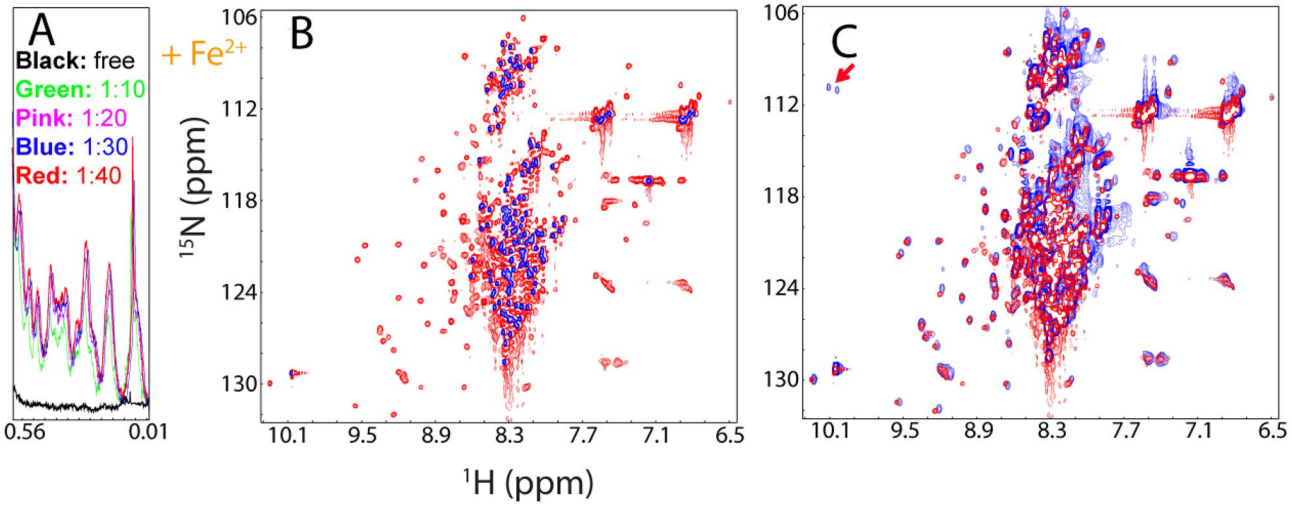

Figure 7. NMR characterization of the interaction of the H80S/D83S hSOD1 with Fe^{2+}. (**A**) Up-field 1D NMR peaks characteristic of H80S/D83S hSOD1 (0.0–0.6 ppm) in the absence and in the presence of Fe^{2+} at different molar ratios. (**B**) Superimposition of HSQC spectra of H80S/D83S-hSOD1 in the absence (blue) and in the presence of Fe^{2+} at a molar ratio of 1:20 (red). (**C**) Superimposition of HSQC spectra of the WT hSOD1 (blue) and H80S/D83S-hSOD1 (red) in the presence of Fe^{2+} at a molar ratio of 1:20.

Human hSOD1 accounts for ~ 1% of the total proteins in neurons. If assuming that the cellular protein concentration is ~ 200 mg/ml, the hSOD1 concentration is ~ 2 mg/ml, or ~ 125 μM. It is well-established that under the physiological conditions, the cellular concentrations of free Fe^{2+} are extremely low as iron is bound to metalloproteins. However, it has been found that in the $SOD1^{G93A}$ mice, the breakdown of blood–spinal cord barrier (BSCB) could result in the availability of free Fe^{2+} in neurons up to 800 ng/mg protein, which is ~ 2.86 mM[31]. That means that free Fe^{2+} concentration is ~ 23 time higher than the SOD1 concentration in neurons. Therefore, here to mimic the in vivo situation, we evaluated the efficiency of Zn^{2+} in triggering the folding of G93A in the pre-existence of Fe^{2+} at ratios (G93A: Fe^{2+}) of 1:10 and 1:25 respectively (Fig. 9C). Interestingly, even in the presence of only 10× Fe^{2+}, the intensity of up-field peaks induced by adding 40× Zn^{2+} is much lower than that without Fe^{2+} (Fig. 9C). Most strikingly, in the pre-existence of 25× Fe^{2+}, addition of 10× zinc is no longer able to induce up-field 1D (Fig. 9C), as well as well-dispersed HSQC peaks (Fig. 9D). Only upon addition of 40× zinc, the up-field peaks manifested to some degree, but however, those peaks are very weak and broad (Fig. 9C). Furthermore, visible aggregates were observed shortly in NMR tube and consequently, no high-quality HSQC spectrum could be acquired on this sample. Although the exact Zn^{2+} concentration in neurons remains to be defined, it was estimated that the Zn^{2+} concentration is only in the 10–30 μM range[50], which is not even reaching

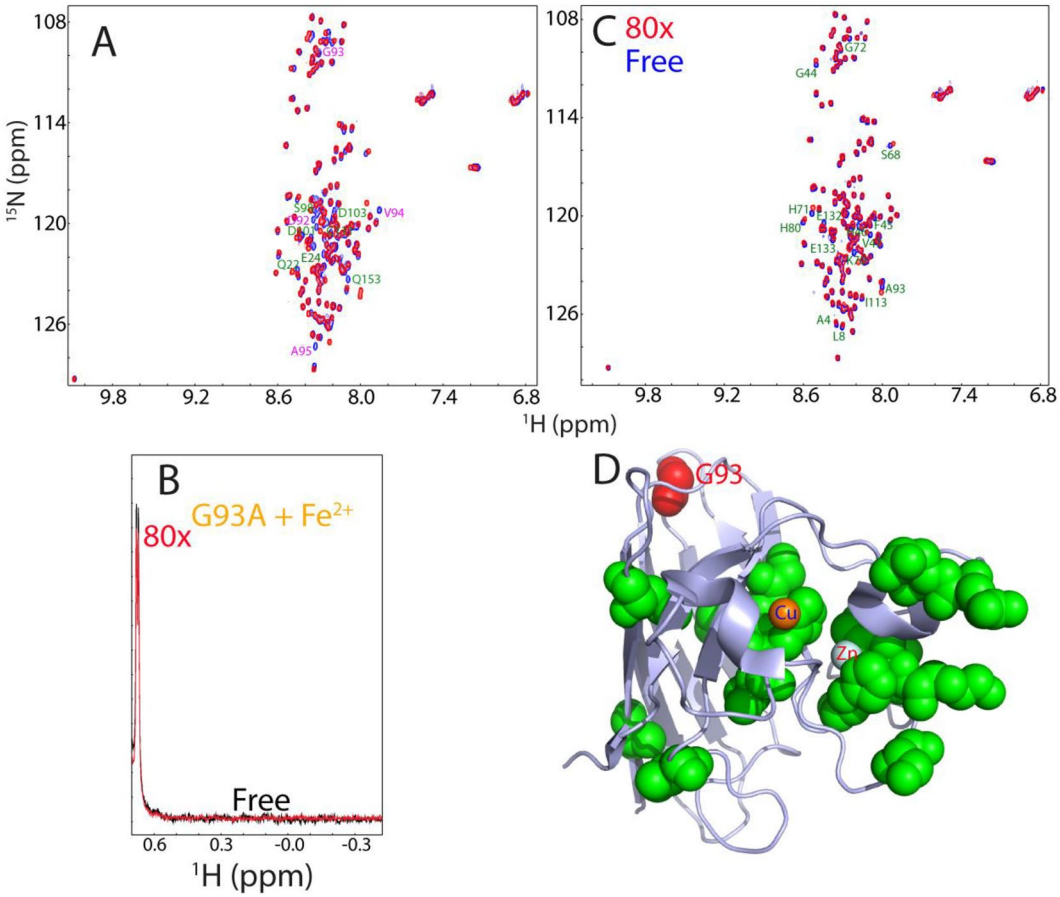

Figure 8. G93A-hSOD1 loses the folding capacity upon induction by Fe^{2+}. (**A**) Superimposition of HSQC spectra of WT (blue) and G96A-hSOD1 (red). Residues with large shifts for their HSQC peaks are labeled. (**B**) Up-field NMR peaks (−0.5 to 0.64 ppm) of G93A-SOD in the absence (black) and in the presence of Fe^{2+} at a molar ratio of 1:80 (red). (**C**) Superimposition of HSQC spectra of G93A-hSOD1 in the absence (blue) and in the presence of Fe^{2+} at a molar ratio of 1:80 (red). Residues with significant shifts for their HSQC peaks are labeled. (**D**) The monomer structure of hSOD1 (1PU0) with the G93A-hSOD1 residues significantly perturbed by Fe^{2+} displayed in green spheres.

a ratio of 1 to 1 with hSOD1. As such, upon the breakdown of the blood–spinal cord barrier, because of the binding of Fe^{2+} to the unfolded G93A-hSOD1 ensemble, the maturation of the G93A-hSOD1 is expected to be significantly retarded in the neurons, consistent with the in vivo observations[5–8,47].

Amyloid formation of hSOD1 under different conditions

Previously, WT hSOD1 has been shown to form amyloid fibrils[51]. Therefore, here, we assessed the amyloid formation of WT hSOD1 in the absence and in the presence of several cations at a 1:20 ratio (hSOD1:cation). We utilized the same methods previously used to characterize the TDP-43 prion-like domain[52] and FUS RRM domain[53] by monitoring ThT-binding induced fluorescence and conducting EM imaging during the 7-day incubation (Fig. S3). Remarkably, the hSOD1 sample in the presence of Zn^{2+} remained transparent throughout the incubation and exhibited no detectable aggregation (II of Fig. S3A) or ThT-binding induced fluorescence (Fig. S3B). On the other hand, hSOD1 samples without any additional cation or with Mg^{2+} incapable of binding nascent hSOD1 aggregated as shown by EM imaging (I and III of Fig. S3A) as well as formed some amyloid-like fibrils, as evidenced by the increase of ThT-binding induced fluorescence (Fig. S3B). Notably, the hSOD1 sample with Cu^{2+} showed a large increase in ThT-binding induced fluorescence on day 3 (Fig. S3B) and amyloid fibrils were clearly visible by EM (IV of Fig. S3A). The hSOD1 sample with Fe^{2+} exhibited a substantial rise in ThT-binding induced fluorescence only on day 5 (Fig. S3B) and also displayed amyloid fibrils under EM imaging, albeit not as distinctly as with Cu^{2+} (V of Fig. S3A). Taken together, the in vitro results here confirm that upon being highly unfolded, WT hSOD1 could indeed form amyloid fibrils[50]. Our results also further suggest that the amyloid formation of hSOD1 appears to be critically influenced by the presence of cations: Zn^{2+} inhibited it, while Cu^{2+} and Fe^{2+} enhanced it.

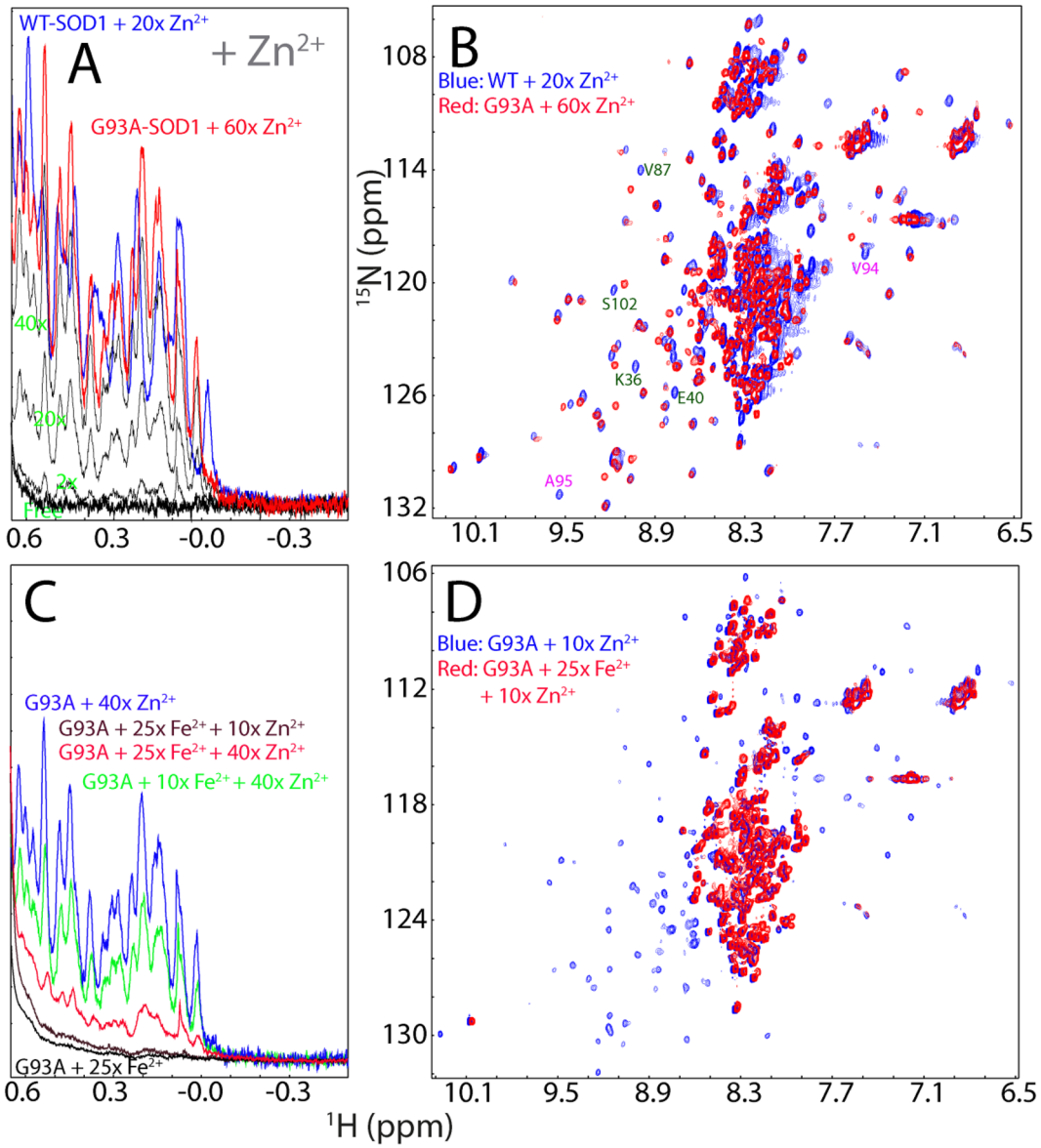

Figure 9. Fe^{2+} reduces the efficiency of the Zn2 + -induced folding of G93A-hSOD1. (**A**) Up-field 1D NMR peaks characteristic of the folded WT or G93A-hSOD1 (− 0.5 to 0.62 ppm) in the presence of Zn^{2+} at different molar ratios. (**B**) Superimposition of HSQC spectra of the WT hSOD1 in the presence of Zn^{2+} at a molar ration of 1:20 (blue), and G93A-hSOD1 in the presence of Zn^{2+} at a molar ration of 1:60 (red). Some residues with large shifts of their HSQC peaks are labeled (**C**) Up-field 1D NMR peaks characteristic of the folded G93A-hSOD1 (− 0.5 to 0.62 ppm) with a pre-existence of 10× or 25× Fe^{2+}, followed by addition of Zn^{2+} at different molar ratios. (**D**) Superimposition of HSQC spectra of G93A-hSOD1 in the presence of 10× Zn^{2+} without (blue) and with the pre-existence of 25× Fe^{2+} (red).

Discussion

In the present study, by a systematic assessment of the effects of 12 cations, we have uncovered several previously-unknown findings. Surprisingly, most of them lack the Zn^{2+}-like ability to both bind and induce folding of nascent hSOD1. In particular, Ni^{2+}, Cd^{2+} and Co^{2+}, which have been widely believed to have physicochemical properties very similar to Zn^{2+} and thus utilized to substitute Zn^{2+} in mature hSOD1 for various biophysical and structural studies[5–7], have no detectable ability to bind as well as to induce the initial folding of nascent hSOD1. Intriguingly, although Cu^{2+}, the catalytic cofactor of hSOD1, shows extensive binding to the unfolded state of hSOD1, it only has weak capacity in inducing folding but owns a strong ability to trigger severe aggregation. Functionally, Zn^{2+} is not essential for the catalytic reaction but appears to critically stabilize the active conformation of the mature hSOD1[5–9]. Here, our current results revealed a new role of Zn^{2+}: to induce the initial folding of nascent hSOD1, which thus provides a potential mechanism for its capacity to switch the toxic nascent hSOD1 into the non-toxic folded state in cells[54]. Indeed, increasing evidence implies that abnormal zinc homeostasis is related

to ALS pathogenesis and to increase the effective cellular concentration of Zn^{2+} such as by the dietary intake might offer an important therapy for ALS patients caused by hSOD1[55,56].

Recently, we found that in addition to the positively-charged Zn^{2+}, the negative-charged ATP and triphosphate could also induce folding of nascent hSOD1 at 1:8 (hSOD1:ATP). By contrast, ADP, Adenosine, pyrophosphate and phosphate, as well as trimethylamine N-oxide (TMAO), the best-known inducer generally for protein folding, showed no detectable inducing capacity at concentrations where aggregation occurred for hSOD1[33]. Nevertheless, unlike the Zn^{2+}-induced folded state, in the ATP-induced folded state, the loop regions around the Cu/Zn-binding pockets remain largely unformed[33]. Therefore, Zn^{2+} appears to be selected by nature to serve as the cofactor of hSOD1 not just because it is a positively charged cation, but it specifically owns a unique integration of at least three abilities: (1) to coordinate the formation of the Zn^{2+}-binding pocket and; (2) to induce folding of nascent hSOD1 as well as; (3) to occupy the pocket of mature hSOD1 to stabilize the conformation of key residues essential for enzymatic catalysis. In this context, while Ni^{2+}, Cd^{2+} and Co^{2+} have the ability to bind the Zn^{2+}-binding pocket in mature hSOD1, they lack the Zn^{2+}-like capacity to induce folding of nascent hSOD1 and to specifically coordinate the formation of the Zn^{2+}-binding pocket. On the other hand, although Cu^{2+} can bind the pocket in mature hSOD1 to serve as a catalytic cofactor as well as extensively bind the unfolded state of nascent hSOD1, it has very weak capacity in inducing folding but exerts a strong adverse effect to trigger severe aggregation. These findings thus may rationalize the observation that the free Cu^{2+} ion is be highly toxic in cells and as such the human copper chaperone for hSOD1 (hCCS) is absolutely needed to carry and then load Cu^{2+} to hSOD1[16–19,30].

We also decode that out of 10 other cations, only Fe^{2+} has the Zn^{2+}-like capacity to induce folding of nascent hSOD1. In particular, the results with WT, H80S/D83S and G93A mutants of hSOD1 reveal that although the Zn^{2+}- and Fe^{2+}-binding pockets are not identical, either binding by Zn^{2+} or Fe^{2+} is sufficient to induce folding of nascent hSOD1. This finding immediately raises an interesting question whether the Fe^{2+}-bound hSOD1 exists or/and functions in any organisms. At present, there is an iron superoxide dismutase (FeSOD), which was first discovered in *E. coli* in 1973[55,56], shortly after the discovery of CuZnSOD in 1969[57] and MnSOD in 1970[58]. FeSOD has now been found in some bacteria, protists, mitochondria and chloroplasts but not in human. In fact, FeSOD is believed to be the first SOD to evolve due to the abundance of iron and low levels of oxygen in Earth's primitive atmosphere. However, structurally FeSOD and MnSOD are almost identical, but fundamentally different from CuZnSOD[59]. As shown in Fig. S4, FeSOD[60] and MnSOD[61] have an identical two-domain structure rich in helices with Fe or Mn atom in the active site, while CuZn-SOD1 has a structure with a beta-barrel and a copper-zinc cluster in the active site.

To the best of our knowledge, so far, there has been no report on detecting any FeSOD with the CuZn-hSOD1 structural fold in any organisms. This raises a question of evolutionary interest: why does nature engineer CuZn-SOD1 which needs two cofactors and multiple steps to reach mature hSOD1 for functionality? In fact, to use Fe^{2+} as the SOD1 cofactor could potentially fulfill both requirements: to initiate folding of nascent hSOD1 and catalyze redox reactions in the mature enzyme. Remarkably, this question might be linked to the Great Oxidation Event[62–64], which occurred approximately 2.4 billion years ago. In this event, cyanobacteria radically altered Earth's atmosphere through the production of molecular oxygen (O_2) as a result of their photosynthetic activity. Previously, it has been suggested that, from an evolutionary perspective, the changes in the metal ions in different SOD enzymes are closely associated with the availability of metal ions on Earth[9,65,66]. More specifically, during the Great Oxidation Event, environmental changes caused by the gradual accumulation of O_2 transformed abundant and soluble Fe^{2+} in the oceans into bio-unavailable iron ore. Simultaneously, it led to the release of soluble Cu^{2+} from copper sulfide ore[65,66]. Consequently, organisms are believed to have adapted to combat superoxide by selecting specific metal ions available in their surroundings[9]. In this context, here we propose that the absence of Fe-SOD with the CuZn-SOD1 fold in organisms might also be due to the unavailability of Fe^{2+} in the environment after the Great Oxidation Event.

Oxidative stress, resulting from an imbalance between the production of free oxidative radicals and the ability of the cell to remove them, has been increasingly identified to cause various human diseases, particularly neurodegenerative diseases[28–31]. In this context, hSOD1 represents a central antioxidative enzyme while iron acts as a notorious accelerator. Iron is a double-edged sword: it is the most abundant "trace element" absolutely required for humans' survival, but high levels of iron quickly lead to cell death. Under the normal conditions, iron is bound with metalloproteins and therefore the cellular concentration of free iron is very low. However, under the pathological conditions such as the breakdown of the blood-central nerve system characteristic of neurodegenerative diseases and aging, the concentration of the blood-derived iron can reach very high[28–31,67–76]. Indeed, iron is accumulated in various neurodegenerative as well as other diseases but the underlying mechanisms for its toxicity still remain to be fully elucidated. Currently, iron is known to trigger oxidative stress mainly through its reactivity with peroxide, thus generating the highly reactive hydroxyl radical by Fenton chemistry[67–73]. Nevertheless, so far, there is no report to imply that iron might manifest its cellular toxicity by specifically targeting SOD1.

Here, the competition experiments of Fe^{2+} and Zn^{2+} reveal that the presence of Fe^{2+} at high concentrations radically reduces the efficiency of the Zn^{2+}-induced folding of both WT and in particular ALS-causing G93A hSOD1. Previously, the failure or even reduced efficiency of the folding has been proposed as a common mechanism for trapping the ALS-causing hSOD1 mutants in the highly-toxic species before the formation of the correct disulfide bridge, which are also prone to aggregation. Consequently, our finding implies a novel SOD1-dependent mechanism for the iron-induced production of oxidative stress by targeting the highly toxic mutants such as G93A, and even WT hSOD1 to disable its anti-oxidative functions. In light of numerous previous results, we propose here a mechanism by which Fe^{2+} targets hSOD1 to provoke oxidative stress as well as to create toxic hSOD1 forms (Fig. 10). More specifically, nascent hSOD1 exists as the unfolded state (Fig. 10A). Only upon supplement of Zn^{2+}, a conformational equilibrium is established in which the folded population is formed (Fig. 10B), thus ready for further interacting with hCCS (Fig. 10C) to reach the mature and active hSOD1 (Fig. 10D) with copper

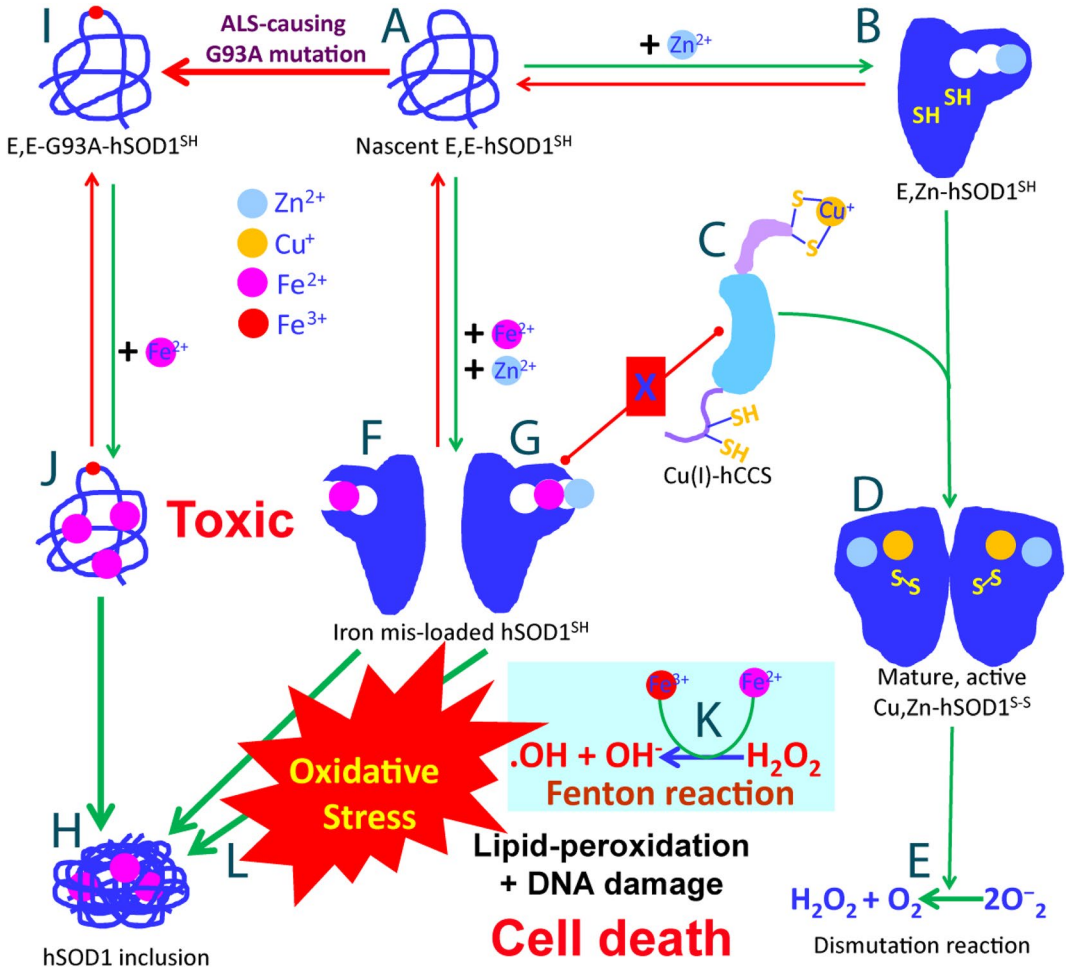

Figure 10. Speculative hSOD1-dependent mechanism by which Fe^{2+} provokes oxidative stress and traps both WT and ALS-causing mutant hSOD1 in the aggregation-prone and toxic forms.

loaded and the disulfide bridge formed capable of catalyzing the dismutation reaction (Fig. 10E). However, if in the presence of Fe^{2+} at high concentrations, even WT-hSOD1 may become the Fe^{2+}-bound, which has an overall architecture similar to the Zn^{2+}-bound (Fig. 10F,G), but unsuitable for further formation of the disulfide bridge and load of copper catalyzed by hCCS. As a consequence, the Fe^{2+}-bound hSOD1 form without the disulfide bridge would ultimately acquire high toxicity as found with other ALS-causing mutants including G93A[47] and H46R/H48Q[48], by becoming aggregated to form the iron-containing hSOD1 inclusion (Fig. 10H) which has been extensively observed in ALS patients.

Specifically, for G93A-hSOD1 causing FALS (Fig. 10I), even without the excess presence of Fe^{2+}, the efficiency of the Zn^{2+}-induced maturation has been demonstrated to be significantly reduced as previously reported[47] as well as observed here by NMR, likely owing to the reduced folding capacity induced by Zn^{2+} (Fig. 9A). This reduction is expected to provoke oxidative stress which may subsequently trigger the breakdown of blood–central nerve system barrier as previously demonstrated on the $SOD1^{G93A}$ mice[31, 72, 75]. Upon the breakdown, the concentration of the blood-derived Fe^{2+} could become as high as ~ 25 times of the hSOD1 concentration. In this context, although Fe^{2+} is no longer able to trigger the folding of G93A-SOD1, it can still bind to a set of residues of the unfolded G93A-hSOD1 ensemble (Fig. 10J) to dramatically disrupt the Zn^{2+}-induced folding, thus blocking the initial folding critical for the G93A-hSOD1 maturation (Fig. 10J). As such, in the presence of Fe^{2+} at high concentration, the immature and disordered G93A-hSOD1 becomes accumulated for forming the iron-containing inclusion as observed in vivo (Fig. 10H). The iron-induced failure of the G93A maturation is expected to aggravate oxidative stress, which might further prompt the breakdown of blood–central nerve system barrier as a positive feedback loop. This mechanism might resolves a long-standing paradox that on the one hand, many mature ALS-causing mutants such as G93A-hSOD1 have their mature structures and activity almost identical to those of the mature WT hSOD1[47], but on the other hand, in vivo they have been found to be highly toxic and aggregation-prone[31, 68, 72].

Our study also raises some interesting issues to be explored in the future. For example, it remains to investigate whether the Fe^{2+}-bound hSOD1, which is chemically similar to Cu^{+}-bound SOD1, also acquires the activity to catalyze endogenous production of nitric oxide to induce apoptosis, as previously detected on the zinc-deficient

hSOD1[47, 48]. Nevertheless, the residue-specific NMR results here unequivocally decipher that in addition to Fenton reaction (Fig. 10K), Fe^{2+} might be also able to manifest its toxicity through a novel SOD1-dependent mechanism, by which Fe^{2+} traps the mutant or even WT hSOD1 into highly toxic forms to provoke significant oxidative stress (Fig. 10L). Both are expected to contribute to pathogenesis of neurodegenerative diseases including ALS as well as aging. This may partly rationalize the observation that under certain pathological conditions, WT hSOD1 is also able to acquire cellular toxicity to initiate ALS. Furthermore, as hSOD1 exists in all human tissues, the SOD1-dependent mechanism found here is expected to play general roles in triggering other diseases upon the bio-availability of free Fe^{2+} at high concentrations in cells. Our study also provides mechanistic supports to the therapeutic approaches to treat neurodegenerative diseases or to slow down aging by repairing the breakdown of the blood-central nerve system barrier[76], or/and intaking iron-chelators by design from EDTA-like compounds or directly from antioxidant natural products such as flavonoids extensively existing in fruits and green tea, which can chelate and clean up Cu^{2+} and Fe^{2+}[77, 78].

Materials and methods

Chemicals and preparation of the recombinant hSOD1 proteins.

Chloride salts of 12 cations were all purchased from Sigma-Aldrich. The gene encoding the wild-type hSOD1 of the native sequence was purchased from Genscript with *E. coli* preferred codons[24, 25]. To remove the inference of extra residues, the gene was subsequently cloned into a modified vector pET28a without any tag[25]. H80S/D83S and G93A mutants were generated by the use of QuikChange Site-Directed Mutagenesis Kit (Stratagene, La Jolla, CA, USA)[33]. Subsequently the expression vector was transformed into and overexpressed in *Escherichia coli* BL21 (DE3) cells (Novagen).

The recombinant WT and mutant hSOD1 proteins were all found in inclusion body. As a result, the pellets were first washed with buffers several times and then dissolved in a phosphate buffer (pH 8.5) containing 8 M urea and 100 mM dithiothreitol (DTT) to ensure complete conversion to Cys-SH. After 1 h, the solution was acidified by adding 10% acetic acid and subsequently purified by reverse-phase (RP) HPLC on a C4 column eluted by water-acetonitrile solvent system[22, 23]. The HPLC elution containing pure recombinant hSOD1 was lyophilized and stored at − 80 degree.

The generation of isotope-labeled proteins for NMR studies followed a similar procedure except that the bacteria were grown in M9 medium with the addition of $(^{15}NH_4)_2SO_4$ for ^{15}N labeling[22, 23, 31]. The purity of the recombinant proteins was checked by SDS–PAGE gels and verified by a Voyager STR matrix-assisted laser desorption ionization time-of-flight-mass spectrometer (Applied Biosystems), as well as NMR assignments. The concentration of protein samples was determined by the UV spectroscopic method in the presence of 8M urea[22, 23, 79].

By exhaustively screening solution conditions including pH, types and concentrations of salts, we have successfully identified the optimized buffer to minimize the aggregation of nascent hSOD1 for high-resolution NMR studies: in 1 mM sodium acetate buffer at pH 4.5. This condition allowed the preparation of soluble and stable hSOD1 samples with a concentration up to 500 μM, which is required to collect high-quality triple-resonance NMR spectra. As hSOD1 of the native sequence contains four cysteine residues, previously we found that they started to form intermolecular disulfide bridges even in the presence of 10 mM DTT once the solution pH was above 5.0, and consequently resulted in immediate precipitation[24, 25]. Indeed, even for the C6A/C111S mutant with a significant reduction of the potential to form intermolecular disulfide bridges, its NMR sample still needed to be prepared at pH 5.0[22]. Here the low buffer-salt concentration (1 mM) was selected also to minimize the potential interference from the buffer cation (Na^+) during titrations of 12 cations. Chloride salts of 12 cations were also dissolved in the same buffer with the final pH value adjusted to 4.5 by very diluted NaOH or HCl.

ITC experiments

Isothermal titration calorimetry (ITC) experiments were performed using a Microcal VP isothermal titration calorimetry machine as described previously[38]. The hSOD1 at a concentration of 5 μM was placed in a 1.8-ml sample cell, and each salt at a concentration of 6 mM were loaded into a 300-μl syringe. The samples were first degassed for 15 min to remove bubbles before the titrations were initiated. Control experiments with the same parameter settings were also performed for each inorganic salt without hSOD1, to subtract the effects because of sample dilution.

NMR experiments

All NMR experiments were acquired at 25 °C on an 800 MHz Bruker Avance spectrometer equipped with pulse field gradient units as described previously[24, 25]. To achieve sequential assignments, triple resonance NMR spectra HN(CO)CACB and CBCA(CO)NH were collected on the ^{15}N-/^{13}C- double labeled hSOD1 samples while {^1H}–^{15}N heteronuclear steady-state NOE (hNOE) and HSQC-NOESY spectra were collected on the ^{15}N-labeled samples. NMR ^1H chemical shifts were referenced to external DSS at 0.0 ppm[15, 16]. NMR spectra were processed with NMR Pipe[80] and analyzed with NMR View[81].

For NMR titrations of 12 cations, ^{15}N-labelled hSOD1 samples at a protein concentration of 50 μM in 1 mM sodium acetate-d3 buffer at pH 4.5 were used with stepwise additions of each cation at molar ratios of 1:0.5, 1:1, 1:2, 1:4, 1:6, 1:8, 1:10, 1:12, 1:16, 1:20, 1:24, 1:30 and 1:40 as well as higher ratios for mutant hSOD1 or Fe^{2+}.

Electron microscopy imaging and ThT-binding induced fluorescence measurements

Incubation samples of the hSOD1 samples at 25 °C at a protein concentration of 20 μM in 1 mM acetate buffer at pH 4.5 were imaged at 3 and 7 days of the incubation in the absence and in the presence of different cations at 1:20 by a TEM microscope (Jeol Jem 2010f. Hrtem, Japan) operating at an accelerating voltage of 200 kV[52, 53]. Briefly, for EM imaging, a 5 μl aliquot of the incubation or aggregate solutions was placed onto the Cu grids (coated

with carbon film; 150 mesh; 3 mm in diameter) and negatively stained with 5 µl of 2% neutral, phosphotungstic acid (PTA). This aliquot was allowed to settle on Cu grid for 30 s before the excess fluid was drained away. The Cu grid was later air-dried for another 15 min before being imaged.

ThT-binding induced fluorescence was measured at 25 °C with a RF-5301 PC spectrophotometer (Shimadzu, Japan) as previously described[52, 53] at different time points of the incubations at 25 °C. For Thioflavin-T (ThT) binding assay, a 2 mM ThT stock solution was prepared by dissolving ThT in milli-Q water and filtered through a 0.22 µm Millipore filter. The fresh working solution was prepared by diluting the stock solution into 1 mM acetate buffer (pH 4.5) to reach a final ThT concentration of 50 µM. A 10 µL aliquot of each incubation solution, or 10 µL aliquot of the incubation buffer (1 mM acetate buffer at pH 4.5) as the control, was mixed with 130 µL of the ThT working solution in the dark for 10 min. The fluorescence emission spectra were acquired for three repeats with the excitation wavelength at 442 nm and slit widths: excitation at 5 nm and emission at 10 nm[53].

Data availability

All data generated or analysed during this study are included in this published article and its supplementary information.

Received: 4 September 2023; Accepted: 12 November 2023
Published online: 14 November 2023

References

1. Bruijn, L. I., Miller, T. M. & Cleveland, D. W. Unraveling the mechanisms involved in motor neuron degeneration in ALS. *Annu. Rev. Neurosci.* **27**, 723–749 (2004).
2. Kiernan, M. C. *et al.* Amyotrophic lateral sclerosis. *Lancet* **377**, 942–955 (2011).
3. Zlokovic, B. V. Neurovascular pathways to neurodegeneration in Alzheimer's disease and other disorders. *Nat. Rev. Neurosci.* **12**, 723–738 (2011).
4. Rosen, D. R. *et al.* Mutations in Cu/Zn superoxide dismutase gene are associated with familial amyotrophic lateral sclerosis. *Nature* **362**, 59–62 (1993).
5. Sheng, Y. *et al.* Superoxide dismutases and superoxide reductases. *Chem. Rev.* **114**, 3854–3918 (2014).
6. Valentine, J. S., Doucette, P. A. & Zittin Potter, S. Copper-zinc superoxide dismutase and amyotrophic lateral sclerosis. *Annu. Rev. Biochem.* **74**, 563–593 (2005).
7. Wright, G. S. A., Antonyuk, S. V. & Hasnain, S. S. The biophysics of superoxide dismutase-1 and amyotrophic lateral sclerosis. *Q. Rev. Biophys.* **52**, e12 (2019).
8. Huai, J. & Zhang, Z. Structural properties and interaction partners of familial ALS-associated SOD1 mutants. *Front. Neurol.* **10**, 527 (2019).
9. Furukawa, Y. Good and bad of Cu/Zn-superoxide dismutase controlled by metal ions and disulfide bonds. *Chem. Lett.* **50**, 331–341 (2021).
10. Chiti, F. & Dobson, C. M. Protein misfolding, functional amyloid, and human disease. *Annu. Rev. Biochem.* **75**, 333–366 (2006).
11. Abel, O. *et al.* ALSoD: A user-friendly online bioinformatics tool for amyotrophic lateral sclerosis genetics. *Hum. Mutat.* **33**, 1345–1351 (2012).
12. Tokuda, E. *et al.* Wild-type Cu/Zn superoxide dismutase is misfolded in cerebrospinal fluid of sporadic amyotrophic lateral sclerosis. *Mol. Neurodegener.* **14**, 42 (2019).
13. Rotunno, M. S. & Bosco, D. A. An emerging role for misfolded wild-type SOD1 in sporadic ALS pathogenesis. *Front. Cell Neurosci.* **7**, 253 (2013).
14. Furukawa, Y. & Tokuda, E. Does wild-type Cu/Zn-superoxide dismutase have pathogenic roles in amyotrophic lateral sclerosis?. *Transl. Neurodegener.* **9**, 33 (2020).
15. Ly, C. V. *et al.* Protein kinetics of superoxide dismutase-1 in familial and sporadic amyotrophic lateral sclerosis. *Ann. Clin. Transl. Neurol.* **10**, 1012–1024 (2023).
16. Furukawa, Y., Torres, A. S. & O'Halloran, T. V. Oxygen-induced maturation of SOD1: A key role for disulfide formation by the copper chaperone CCS. *EMBO J.* **23**, 2872–2881 (2004).
17. Banci, L. *et al.* Human superoxide dismutase 1 (hSOD1) maturation through interaction with human copper chaperone for SOD1 (hCCS). *Proc. Natl. Acad. Sci. U. S. A.* **109**, 13555–13560 (2012).
18. Banci, L. *et al.* Atomic-resolution monitoring of protein maturation in live human cells by NMR. *Nat. Chem. Biol.* **9**, 297–299 (2013).
19. Luchinat, E. *et al.* In-cell NMR reveals potential precursor of toxic species from SOD1 fALS mutants. *Nat. Commun.* **5**, 5502 (2014).
20. Arnesano, F. *et al.* The unusually stable quaternary structure of human Cu, Zn-superoxide dismutase 1 is controlled by both metal occupancy and disulfide status. *J. Biol. Chem.* **279**, 47998–48003 (2004).
21. Furukawa, Y. *et al.* Conformational disorder of the most immature Cu, Zn-superoxide dismutase leading to amyotrophic lateral sclerosis. *J. Biol. Chem.* **291**, 4144–4155 (2016).
22. Banci, L. *et al.* Human SOD1 before harboring the catalytic metal: Solution structure of copper-depleted, disulfide-reduced form. *J. Biol. Chem.* **281**, 2333–2337 (2006).
23. Sekhar, A. *et al.* Thermal fluctuations of immature SOD1 lead to separate folding and misfolding pathways. *Elife* **4**, e07296 (2015).
24. Lim, L., Lee, X. & Song, J. Mechanism for transforming cytosolic SOD1 into integral membrane proteins of organelles by ALS-causing mutations. *Biochim. Biophys. Acta* **1848**, 1–7 (2015).
25. Lim, L. & Song, J. SALS-linked WT-SOD1 adopts a highly similar helical conformation as FALS-causing L126Z-SOD1 in a membrane environment. *Biochim. Biophys. Acta* **1858**, 2223–2230 (2016).
26. Sun, S. *et al.* Translational profiling identifies a cascade of damage initiated in motor neurons and spreading to glia in mutant SOD1-mediated ALS. *Proc. Natl. Acad. Sci. U. S. A.* **112**, E6993-7002 (2015).
27. Sannigrahi, A. *et al.* The metal cofactor zinc and interacting membranes modulate SOD1 conformation-aggregation landscape in an in vitro ALS model. *Elife* **10**, e61453 (2021).
28. Kwan, J. Y. *et al.* Iron accumulation in deep cortical layers accounts for MRI signal abnormalities in ALS: Correlating 7 tesla MRI and pathology. *PLoS ONE* **7**, e35241 (2012).
29. Ignjatović, A., Stević, Z., Lavrnić, S., Daković, M. & Bačić, G. Brain iron MRI: A biomarker for amyotrophic lateral sclerosis. *J. Magn. Reson. Imaging* **38**, 1472–1479 (2013).
30. Tokuda, E. & Furukawa, Y. Copper homeostasis as a therapeutic target in amyotrophic lateral sclerosis with SOD1 mutations. *Int. J. Mol. Sci.* **17**(5), 636 (2016).
31. Winkler, E. A. *et al.* Blood-spinal cord barrier disruption contributes to early motor-neuron degeneration in ALS-model mice. *Proc. Natl. Acad. Sci. U. S. A.* **111**, E1035–E1042 (2014).

32. Fraga, C. G. Relevance, essentiality and toxicity of trace elements in human health. *Mol. Aspects Med.* **26**, 235–244 (2005).
33. Kang, J., Lim, L. & Song, J. ATP induces folding of ALS-causing C71G-hPFN1 and nascent hSOD1. *Commun. Chem.* **2**, 223 (2023).
34. Deng, H. X. *et al.* Conversion to the amyotrophic lateral sclerosis phenotype is associated with intermolecular linked insoluble aggregates of SOD1 in mitochondria. *Proc. Natl. Acad. Sci. U. S. A.* **103**, 7142–7147 (2006).
35. Furukawa, Y. *et al.* Disulfide cross-linked protein represents a significant fraction of ALS-associated Cu, Zn-superoxide dismutase aggregates in spinal cords of model mice. *Proc. Natl. Acad. Sci. U. S. A.* **103**, 7148–7153 (2006).
36. Toichi, K., Yamanaka, K. & Furukawa, Y. Disulfide scrambling describes the oligomer formation of superoxide dismutase (SOD1) proteins in the familial form of amyotrophic lateral sclerosis. *J. Biol. Chem.* **288**, 4970–4980 (2013).
37. Dyson, H. J. & Wright, P. E. Unfolded proteins and protein folding studied by NMR. *Chem. Rev.* **104**(8), 3607–3622 (2004).
38. Strange, R. W. *et al.* Variable metallation of human superoxide dismutase: atomic resolution crystal structures of Cu-Zn, Zn-Zn and as-isolated wild-type enzymes. *J. Mol. Biol.* **356**, 1152–1162 (2006).
39. Zhang, O., Kay, L. E., Olivier, J. P. & Forman-Kay, J. D. Backbone 1H and 15N resonance assignments of the N-terminal SH3 domain of drk in folded and unfolded states using enhanced-sensitivity pulsed field gradient NMR techniques. *J. Biomol. NMR* **4**(6), 845–858 (1994).
40. Qin, H., Lim, L. Z. & Song, J. Dynamic principle for designing antagonistic/agonistic molecules for EphA4 receptor, the only known ALS modifier. *ACS Chem. Biol.* **10**, 372–378 (2015).
41. Qin, H., Lim, L. Z., Wei, Y. & Song, J. TDP-43 N terminus encodes a novel ubiquitin-like fold and its unfolded form in equilibrium that can be shifted by binding to ssDNA. *Proc. Natl. Acad. Sci. U. S. A.* **111**, 18619–18624 (2014).
42. Palmer, A. G., Kroenke, C. D. & Loria, J. P. Nuclear magnetic resonance methods for quantifying microsecond-to-millisecond motions in biological macromolecules. *Methods Enzymol.* **339**, 204–238 (2001).
43. Roberts, B. R. *et al.* Structural characterization of zinc-deficient human superoxide dismutase and implications for ALS. *J. Mol. Biol.* **373**, 877–890 (2007).
44. Williamson, M. P. Using chemical shift perturbation to characterise ligand binding. *Prog. Nucl. Magn. Reson. Spectrosc.* **73**, 1–16 (2013).
45. Kang, J., Lim, L. & Song, J. ATP binds and inhibits the neurodegeneration-associated fibrillization of the FUS RRM domain. *Commun. Biol.* **2**, 223 (2019).
46. Kayatekin, C., Zitzewitz, J. A. & Matthews, C. R. Zinc binding modulates the entire folding free energy surface of human Cu, Zn superoxide dismutase. *J Mol Biol.* **384**, 540–555 (2008).
47. Galaleldeen, A. *et al.* Structural and biophysical properties of metal-free pathogenic SOD1 mutants A4V and G93A. *Arch. Biochem. Biophys.* **492**, 40–47 (2009).
48. Winkler, D. D. *et al.* Structural and biophysical properties of the pathogenic SOD1 variant H46R/H48Q. *Biochemistry* **48**, 3436–3447 (2009).
49. Otting, G. Protein NMR using paramagnetic ions. *Annu. Rev. Biophys.* **39**, 387–405 (2010).
50. Frederickson, C. J., Koh, J. Y. & Bush, A. I. The neurobiology of zinc in health and disease. *Nat. Rev. Neurosci.* **6**, 449–462 (2005).
51. Furukawa, Y., Kaneko, K., Yamanaka, K., O'Halloran, T. V. & Nukina, N. Complete loss of post-translational modifications triggers fibrillar aggregation of SOD1 in the familial form of amyotrophic lateral sclerosis. *J. Biol. Chem.* **283**, 24167–24176 (2008).
52. Lim, L., Wei, Y., Lu, Y. & Song, J. ALS-causing mutations significantly perturb the self assembly and interaction with nucleic acid of the intrinsically disordered prion-like domain of TDP-43. *PLoS Biol.* **14**, e1002338 (2016).
53. Lu, Y., Lim, L. & Song, J. RRM domain of ALS/FTD-causing FUS characteristic of irreversible unfolding spontaneously self-assembles into amyloid fibrils. *Sci. Rep.* **7**, 1043 (2017).
54. Homma, K. *et al.* SOD1 as a molecular switch for initiating the homeostatic ER stress response under zinc deficiency. *Mol. Cell* **52**, 75–86 (2013).
55. Lopes da Silva, H. F. *et al.* Dietary intake and zinc status in amyotrophic lateral sclerosis patients. *Nutr. Hosp.* **34**, 1361–1367 (2017).
56. Yost, F. J. & Fridovich, I. An Iron-containing superoxide dismutase from *Escherichia coli*. *Biol. Chem.* **248**, 4905–4908 (1973).
57. McCord, J. M. & Fridovich, I. Superoxide dismutase. An enzymic function for erythrocuprein (hemocuprein). *J. Biol. Chem.* **244**, 6049–6055 (1969).
58. Keele, B. B. Jr., McCord, J. M. & Fridovich, I. Superoxide dismutase from *Escherichia coli* B. A new manganese-containing enzyme. *J. Biol. Chem.* **245**, 6176–6181 (1970).
59. Stallings, W. C., Pattridge, K. A., Strong, R. K. & Ludwig, M. L. Manganese and iron superoxide dismutases are structural homologs. *J. Biol. Chem.* **259**, 10695–10699 (1984).
60. Lah, M. S. *et al.* Structure-function in *Escherichia coli* iron superoxide dismutase: Comparisons with the manganese enzyme from Thermus thermophilus. *Biochemistry* **34**, 1646–1660 (1995).
61. Borgstahl, G. E., Pokross, M., Chehab, R., Sekher, A. & Snell, E. H. Cryo-trapping the six-coordinate, distorted-octahedral active site of manganese superoxide dismutase. *J. Mol. Biol.* **296**, 951–959 (2000).
62. Bekker, A. *et al.* Dating the rise of atmospheric oxygen. *Nature* **427**, 117 (2004).
63. Lyons, T. W., Reinhard, C. T. & Planavsky, N. J. The rise of oxygen in Earth's early ocean and atmosphere. *Nature* **506**, 307–315 (2014).
64. Canfield, D. E. *et al.* Oxygen dynamics in the aftermath of the Great Oxidation of Earth's atmosphere. *Proc. Natl Acad. Sci. USA* **110**, 16736–16741 (2013).
65. Saito, M. A., Sigman, D. M. & Morel, F. M. M. The bioinorganic chemistry of the ancient ocean: The co-evolution of cyanobacterial metal requirements and biogeochemical cycles at the Archean-Proterozoic boundary?. *Inorg. Chim. Acta* **356**, 308 (2003).
66. Dupont, C. L., Butcher, A., Valas, R. E., Bourne, P. E. & Caetano-Anollés, G. History of biological metal utilization inferred through phylogenomic analysis of protein structures. *Proc. Natl. Acad. Sci. U.S.A.* **107**, 10567 (2010).
67. Andrews, N. C. & Schmidt, P. J. Iron homeostasis. *Annu. Rev. Physiol.* **69**, 69–85 (2007).
68. Montagne, A. *et al.* Blood-brain barrier breakdown in the aging human hippocampus. *Neuron* **85**, 296–302 (2015).
69. Halliwell, B. & Gutteridge, J. M. C. *Free Radicals in Biology and Medicine* 3rd edn. (Oxford University Press, 1999).
70. Simonian, N. A. & Coyle, J. T. Oxidative stress in neurodegenerative diseases. *Annu. Rev. Pharmacol. Toxicol.* **36**, 83–106 (1996).
71. Barber, S. C., Mead, R. J. & Shaw, P. J. Oxidative stress in ALS: A mechanism of neurodegeneration and a therapeutic target. *Biochim. Biophys. Acta* **1762**, 1051–1067 (2006).
72. Winkler, E. A. *et al.* Blood-spinal cord barrier disruption contributes to early motor-neuron degeneration in ALS-model mice. *Proc. Natl. Acad. Sci. U. S. A.* **111**, E1035–E1042 (2014).
73. Rouault, T. A. Iron metabolism in the CNS: implications for neurodegenerative diseases. *Nat. Rev. Neurosci.* **14**, 551–564 (2013).
74. Joppe, K. *et al.* The contribution of iron to protein aggregation disorders in the central nervous system. *Front. Neurosci.* **13**, 15 (2019).
75. Montagne, A. *et al.* Blood-brain barrier breakdown in the aging human hippocampus. *Neuron* **85**, 296–302 (2015).
76. Ronaldson, P. T. & Davis, T. P. Targeting transporters: Promoting blood-brain barrier repair in response to oxidative stress injury. *Brain Res.* https://doi.org/10.1016/j.brainres.2015.03.018 (2015).
77. Wang, X. *et al.* Role of flavonoids in the treatment of iron overload. *Front. Cell Dev. Biol.* **9**, 685364 (2021).
78. Rodríguez-Arce, E. & Saldías, M. Antioxidant properties of flavonoid metal complexes and their potential inclusion in the development of novel strategies for the treatment against neurodegenerative diseases. *Biomed. Pharmacother.* **143**, 112236 (2021).
79. Pace, C. N. *et al.* How to measure and predict the molar absorption coefficient of a protein. *Protein Sci.* **4**, 2411–2423 (1995).

80. Delaglio, F. *et al.* NMRPipe: A multidimensional spectral processing system based on UNIX pipes. *J. Biomol. NMR* **6**, 277–293 (1995).
81. Johnson, B. A. & Blevins, R. A. NMR view: A computer program for the visualization and analysis of NMR data. *J. Biomol. NMR* **4**, 603–614 (1994).

Acknowledgements
This study is supported by Ministry of Education of Singapore MOE Tier 1 A-8000711-00-00 Grant to Jianxing Song.

Author contributions
J.S. designed research; L. L., J. K. and J.S. performed research; L.L., J. K. and J.S. analyzed data; J.S. wrote the paper.

Competing interests
The authors declare no competing interests.

Additional information
Supplementary Information The online version contains supplementary material available at https://doi.org/10.1038/s41598-023-47338-8.

Correspondence and requests for materials should be addressed to J.S.

Reprints and permissions information is available at www.nature.com/reprints.

Publisher's note Springer Nature remains neutral with regard to jurisdictional claims in published maps and institutional affiliations.